International Conference on Space Optics—ICSO 2018

Chania, Greece

9–12 October 2018

Edited by Zoran Sodnik, Nikos Karafolas, and Bruno Cugny

Straylight analysis on ASPIICS, PROBA-3 coronagraph

C. Galy

C. Thizy

Y. Stockman

D. Galano

et al.

International Conference on Space Optics — ICSO 2018, edited by Zoran Sodnik, Nikos Karafolas, Bruno Cugny, Proc. of SPIE Vol. 11180, 111802H · © 2018 ESA and CNES · CCC code: 0277-786X/18/$18 · doi: 10.1117/12.2536008

Straylight analysis on ASPIICS, PROBA-3 coronagraph

Galy C [1], Thizy C [1], Stockman Y [1], Galano D [2], Rougeot R [2], Melich R [3], Shestov S [4], Landini F [5], Zukhov A [4], Kirschner V [2], Horodyska P [3], Fineschi S [5]

[1] Centre Spatial De Liège (CSL), Liège, Belgium
[2] ESTEC – European Space Research and Technology Centre, Noordwijk, Netherlands
[3] Institute of Plasma Physics ASCR v.v. i. (TOPTEC), Turnov, Czech Republic
[4] Solar-Terrestrial Center of Excellence (SIDC), Royal Observatory of Belgium, Brussels, Belgium
[5] INAF – Astrophysical Observatory of Torino, Torino, Italy

ABSTRACT

PROBA-3 is a mission devoted to the in-orbit demonstration (IOD) of precise formation flying (F^2) techniques and technologies for future ESA missions. The mission includes two spacecraft. One of them will act as an external occulter for scientific observations of the solar corona from the other spacecraft, which will hold the ASPIICS coronagraph instrument, under CSL responsibility.

The ASPIICS instrument on PROBA-3 looks at the solar corona through a refractive telescope, able to select 3 different spectral bands: Fe XIV line @ 530.4nm, He I D3 line @587.7nm, and the white-light spectral band [540;570nm]. The external occulter being located at ~ 150 meters from the instrument entrance, will allow ASPIICS to observe the corona really close to the solar limb, probably closer than any internally or externally occulted coronagraph ever observed.

This paper will present the straylight model and analyses carried out by CSL. A first specificity of the analysis is that the scene on the useful Field of View (FOV) is the solar corona which has a brightness dynamic range as high as 10^3 between the close corona, close to 1 solar radius (Rsun), and the "distant" corona around 3RSun. The specifications are very stringent for this type of instrument. A consensus was found and will be presented regarding the expected straylight within the FOV. It will also be shown that to achieve realistic estimations it is required to take into account the exact location of the created straylight as well as the entrance field.

The second specificity that had to be analyzed is that the diffraction from the solar disk by the external occulter enters the instrument un-obstructed until the internal occulter, and with a brightness 100 times higher than the close corona (~1RSun) brightness. The simulation of this diffraction as well as its propagation inside the ASPIICS telescope creating additional straylight, had to be carefully established in order to give realistic results of its impact on the performances while being actually possible to compute.

Keywords: ASPIICS, Coronagraph, Formation Flying, External Occulter, Straylight, CSL

1. INTRODUCTION

PROBA-3 is a mission devoted to the in-orbit demonstration (IOD) of precise formation flying (F^2) techniques and technologies for future ESA missions. It is part of the overall ESA IOD strategy and it is implemented by the Directorate of Technical and Quality management (D/TEC) under a dedicated element of the General Support Technology Programme (GSTP). The evolution of the design and achievements are presented in [3], [4], [6] and [10].

PROBA-3 will fly ASPIICS (Association of Spacecraft for Polarimetric and Imaging Investigation of the Corona of the Sun) as primary payload, which makes use of the formation flying technique to form a giant coronagraph capable of producing a nearly perfect eclipse allowing observing the sun corona closer to the rim than ever before. The coronagraph system is distributed over two satellites flying in formation (approx. 150m apart). The so called Coronagraph SpaceCraft (CSC) carries the camera and the so called Occulter SpaceCraft (OSC) carries the sun occulter disc.

A secondary payload will be embarked on the occulter satellite; it consists of the DARA solar radiometer.

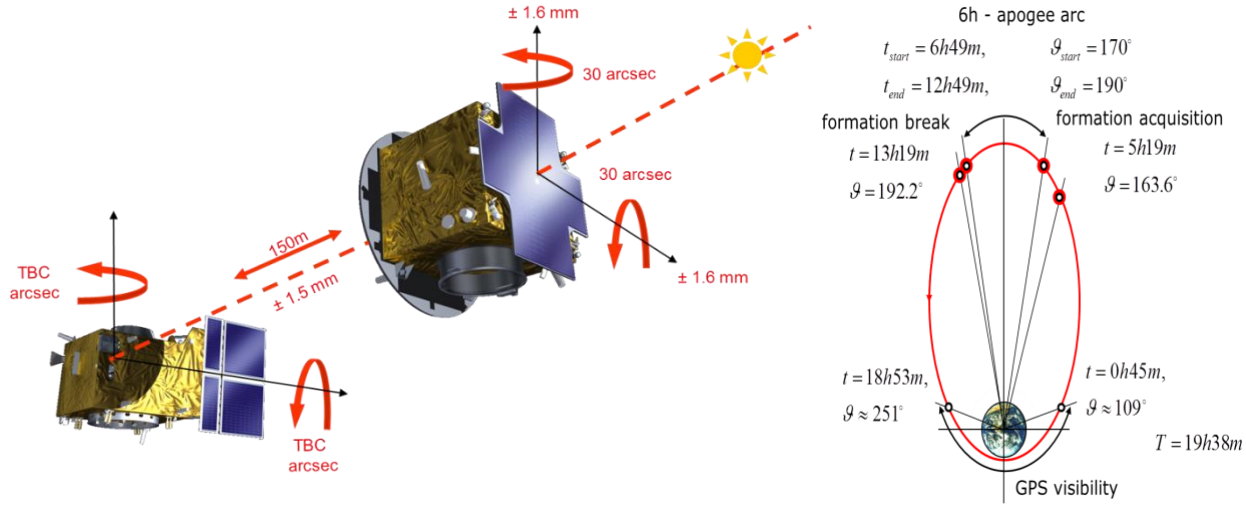

Figure 1. PROBA-3 formation flying overview and orbit.

The science objectives of the mission are presented in [1], [1]. These are basically the observation of the solar corona in an area close to 1 solar radius, where the magnetic field plays a crucial role in the coronal dynamics, thus providing continuous observational conditions very close to those during a total solar eclipse, but without the effects of the Earth's atmosphere.

The proposed PROBA-3 Coronagraph System (ASPIICS) will be the first space coronagraph to cover the range of radial distances between 1.08 and 3 solar radii. ASPIICS will combine observations of the corona in white light and polarization brightness with images of prominences in the He I 5877 Å line and in the Fe XIV 5304 Å line.

ASPIICS will provide novel solar observations to achieve the two major solar physics science objectives: to understand physical processes that govern the quiescent solar corona, and to understand physical processes that lead to coronal mass ejections (CMEs) and determine space weather.

The PROBA-3 coronagraph optical design follows the general principles of a classical externally occulted Lyot coronagraph. The external occulter (EO), hosted by the Occulter Spacecraft (OSC), blocks the light from the solar disc while the coronal light passes through the circular entrance aperture of the Coronagraph Optical Box (COB), accommodated on the Coronagraph Spacecraft (CSC).

1.1 ASPIICS Model

Optical Model

The optical design of ASPIICS and its performances are presented in [5].

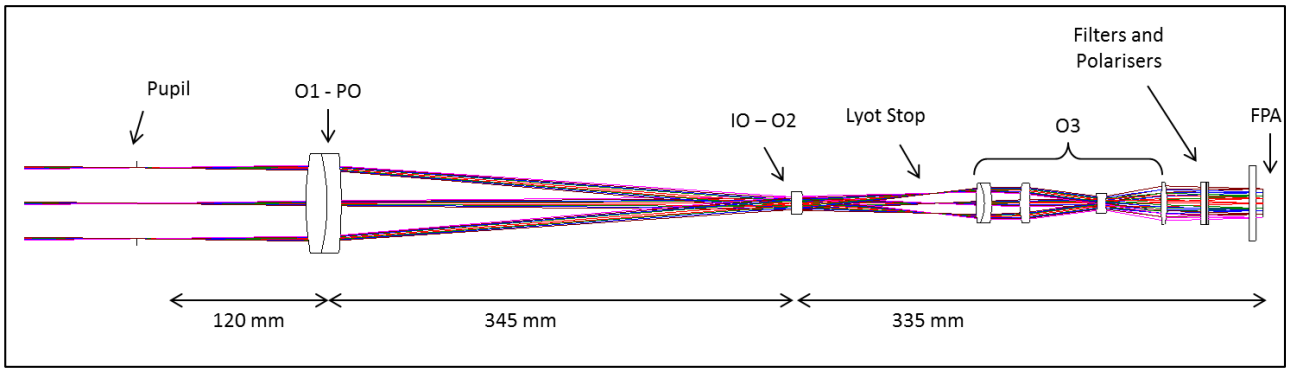

Figure 2 - Optical Model v15.2

It is composed of 4 single lenses, 2 doublet lenses, 1 window, 1 glass stack symbolizing the filters and polarizers, a Lyot stop and the internal occulter (IO) coated on the O2 lens. The window in front of the FPA comprises a 50% neutral density as a mean to reduce the ghosts. It will be seen in the ghost analysis here below that most of the remaining ghosts related to the filter comes from reflections between the two faces of the filter.

Mechanical Model

The mechanical model is shown in Figure 3. The stray light baffle is a long tube (more than 500 mm) between the entrance pupil and the box containing the optics with a diameter of 121 mm. The primary objective made of 2 lenses is placed inside the tube 120 mm away from the entrance pupil. The shadow position sensor (SPS) is placed inside the baffle behind the entrance pupil and presents a thickness of 39.8 mm. Some vanes are placed inside the baffle to stop stray light.

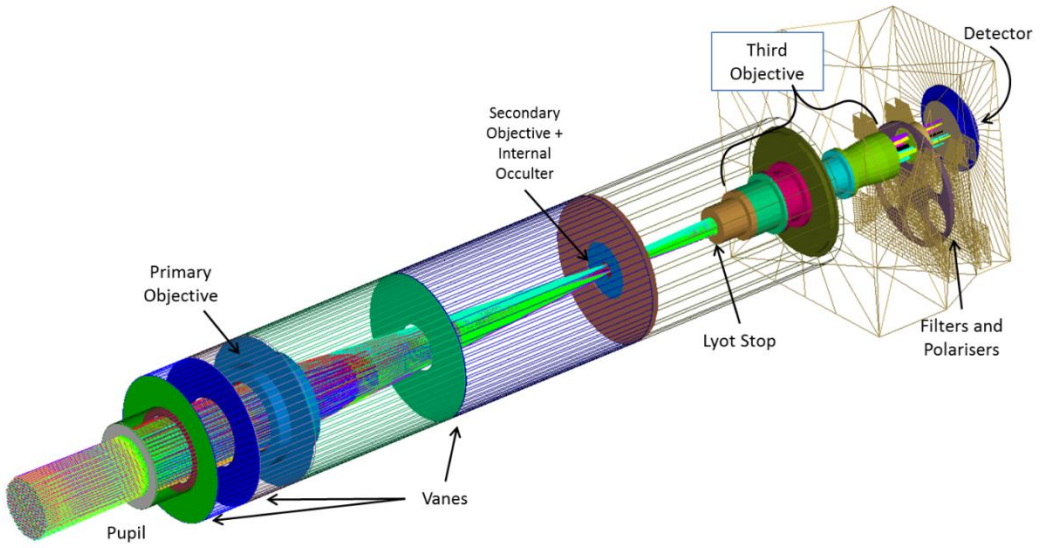

Figure 3 - Mechanical Model

Coatings

For the analysis, measurements of antireflection coatings reflection made by TOPTEC (CZ) are considered on each surface. The PO first lens front surface is not coated and presents a natural reflectivity of 4%. Figure 4 below illustrates two reflection measurements made on the demonstration model (DM) lense.

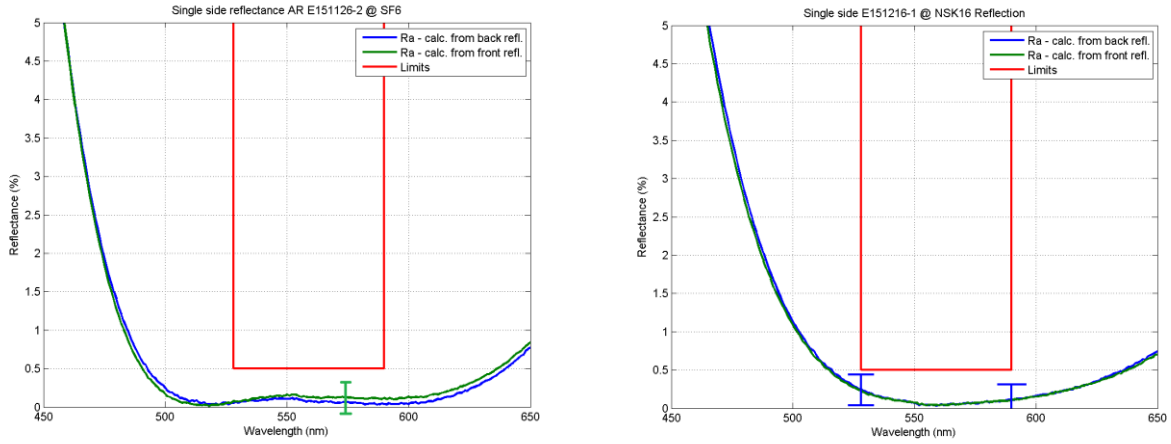

Figure 4 - Antireflection coating measurements (DM Lenses)

Concerning the filters, the ghosts' analysis showed that the initial wide band filter (WBF) created too much ghost straylight. It was decided to change for another company, Optics Balzers Jena (OBJ), which provided really good wide band filters for the SENTINEL 2 program. For the following analysis, the reflectivity taken into account for the WBF is the preliminary design provided by OBJ. Figure 5 below shows a comparison of the previous filter with the new WBF baseline from OBJ.

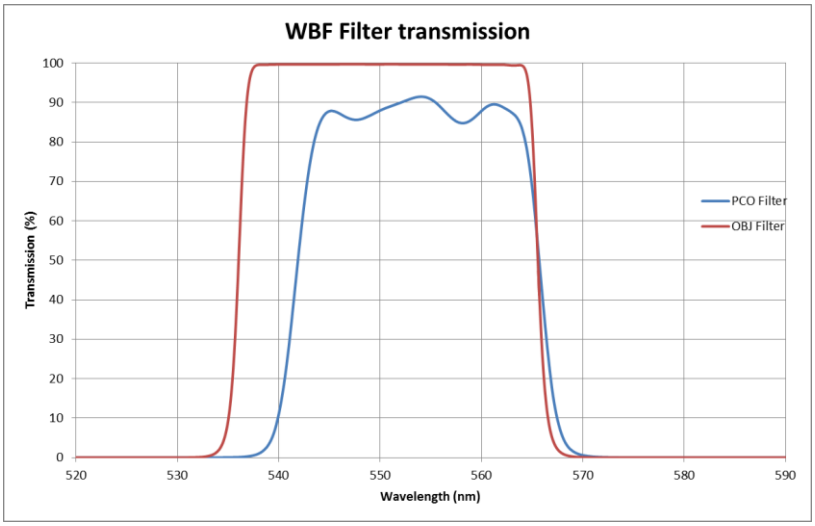

Figure 5 - Comparison of previous and new WBF transmission.

The ASPIICS instrument ultimately aims to observe the solar corona through the He I D3 and the Fe XIV line. However, this article will only present results for the wide band filter channel due to insufficient data on the other filters at the time.

Concerning the detector, reflectivity measurements were performed in order to characterize this second cause of ghosts straylight. Figure 6 shows the reflectivity curve. For the analysis, an equivalent reflectivity is taken into account depending on the spectral range of operation. For the WBF channel, this reflectivity was taken at 15%.

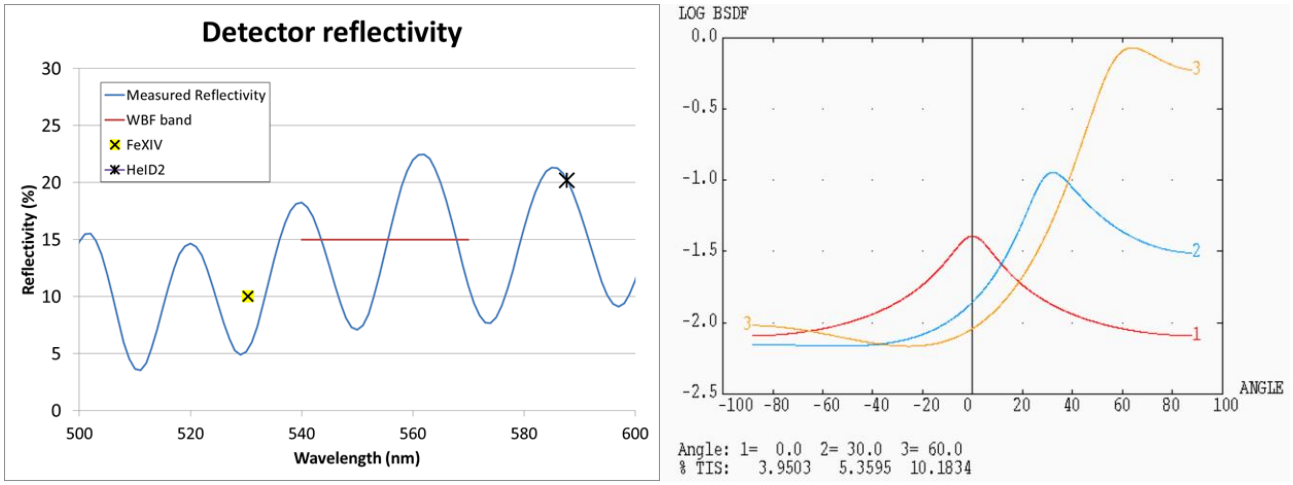

Figure 6 - Detector reflectivity measurement (left) and BSDF model of the anodized black coating (right)

For the mechanical elements a black coating corresponding to a standard black anodizing is considered.

The model has been retrieved from a previous project called OLCI for which it had been validated with scattering measurements. The BSDF model is shown on Figure 6 above. The total internal scattering (TIS) at normal incidence is 3.95 %.

1.2 Context

The specificity of the instrument is that the scene on the useful FoV is the solar corona which can have a brightness dynamic range as high as 10^3 between the close corona (close to 1RSun) and the "far" corona around 3RSun. This specificity was neither well pointed out through the requirement document nor carefully taken into account during the previous straylight analyses for ASPIICS. This is however a strong driver of the importance that one should give to the different process of straylight occurring in the instrument.

While we generally focus on the total amount of straylight on the detector for a given FoV in usual instruments, a strong dynamic range in the observed scene needs the analysis to also focus on where the straylight hit the detector and compare the straylight coming from each source to the signal at this specific location on the detector. Figure 7 below illustrates the need to take into account the exact location of the created straylight as well as the entrance field to make realistic estimations.

This specificity affects the ghost images that are out-of-focus multi-reflection that can be more or less concentrated on different parts of the detector, but also diffuse straylight that is generally homogeneous on the detector (i.e. due to the lens surfaces micro-roughness) because one pixel on the detector will cumulate the effect of scattering by each part of the corona. There are different ways to propagate unwanted straylight inside an instrument. What is relevant for this instrument are the following:

- Multi-reflections (ghosts) on the optical surfaces
- Scattering (by the optics, by the structure …)
- Diffraction (from solar disk on Occulter edges, on the pupil's edge …) (multi-reflections and scattering of this diffraction as well)

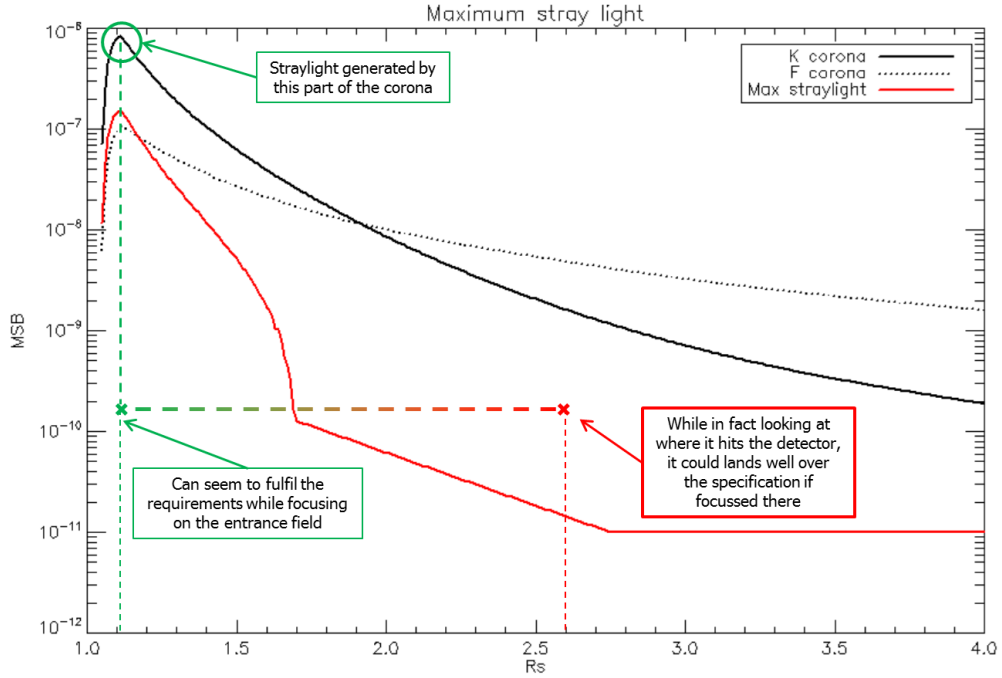

Figure 7 - Illustration of the instrument specificity in terms of straylight

That being said, it is now necessary to define the different sources of straylight and their effect on the analysis. The straylight sources can be separated in 2 general types of sources: sources in the field of view (FoV) of the instrument and sources out of the FoV. This paper will focus on in-FoV straylight sources which are the most critical sources for ASPIICS. The in-FoV sources that generate straylight inside the FoV and for which ghosts and scattering should be calculated are:

1- Solar corona
2- Optical Positioning Sensors Emitters (OPSE)
3- External occulter diffraction

1.3 Specification

The initial specification as expressed in the previous paragraph is shown on the Figure 8 below. As explained earlier, this expression of the straylight level is not clearly representative of the reality of the straylight level at the detector level.

The RSun value of the abscissa is taken into account in the analysis as the RSun coordinate on the detector. But the K-Corona itself is expressed with respect to the entrance fields.

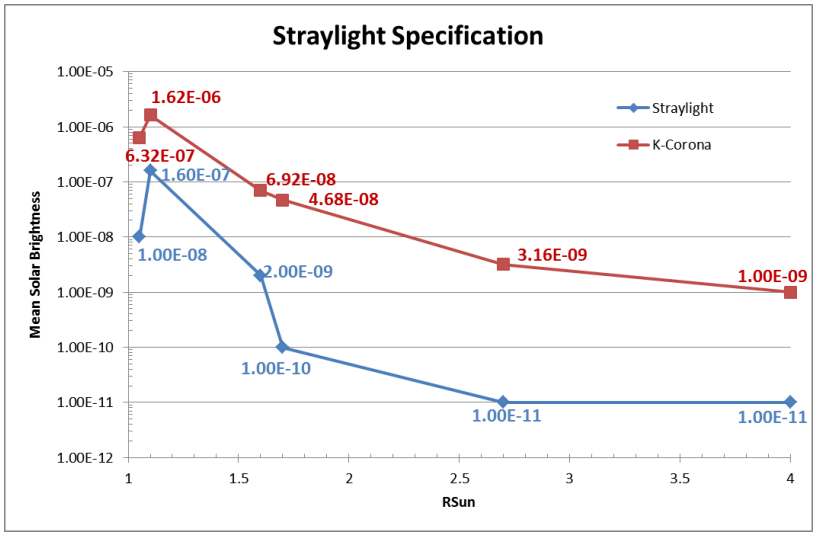

Figure 8 - Straylight Specification

Instead of expressing the K-Corona and the straylight level in MSB, it was decided for the analysis to express the maximum straylight level in term of corona brightness percentage. Figure 9 below show the translation that was made to the specification. That way, all results should be expressed in terms of corona brightness percentage with respect to their location on the detector and can then be compared to the specification.

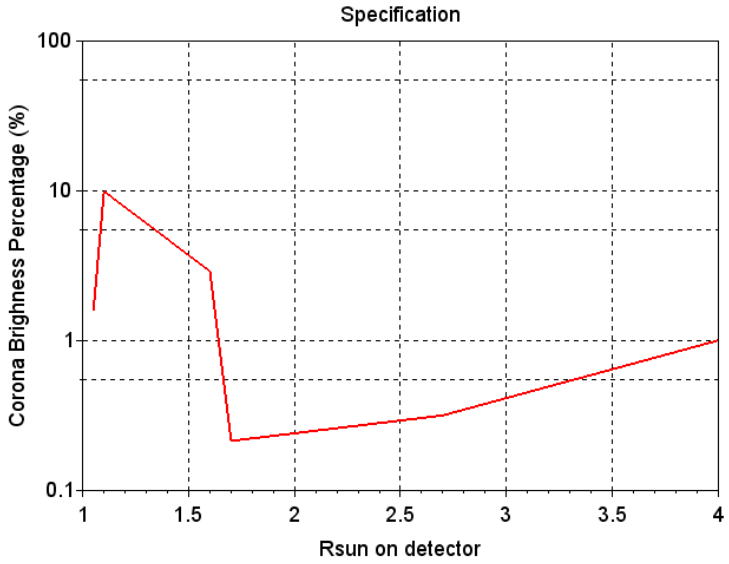

Figure 9 - Translation of the specification in corona brightness percentage

1.4 Use of the specification: Model

As seen on previous paragraphs, the maximum straylight requirement is a function of the RSun radius (radial distance from the sun center).

Usually, in straylight requirements and analysis, the concern is focused on the incoming field angle. This leads to calculating the PST (Point Source Transmittance) which is a transfer function relating the irradiance at the focal plane due to straylight mechanisms to the irradiance at the entrance aperture of the telescope produced by a distance point source. Considering the specificity of the observed signal, it appeared that this definition of the straylight would need too much time to implement, while not being fully representative of the reality of the straylight. It was then decided to compute the whole K-Corona irradiance profile on the entrance aperture (angular and intensity characteristic) in order to be able to combine the effect of the straylight created by each angular filed to another.

This way allowed seeing quite fast that there was a need to have better filters and to find other solution to limit the ghosts' intensity.

The corona intensity is set up in ASAP™ software as the irradiance distribution of the source. The whole corona irradiance is then propagated through ASPIICS in order to calculate the ghosts and scattering associated with this signal (In-Field straylight). Figure 10 below shows the K-Corona irradiance distribution at the entrance pupil, expressed in Mean Solar Brightness (MSB)

In order to calculate the complete straylight level and compare to the specification, all the other sources of straylight have to be expressed as irradiance at the entrance pupil, in MSB. The propagation of these sources inside the instrument will then give an irradiance on the detector that will be comparable to that of the solar corona

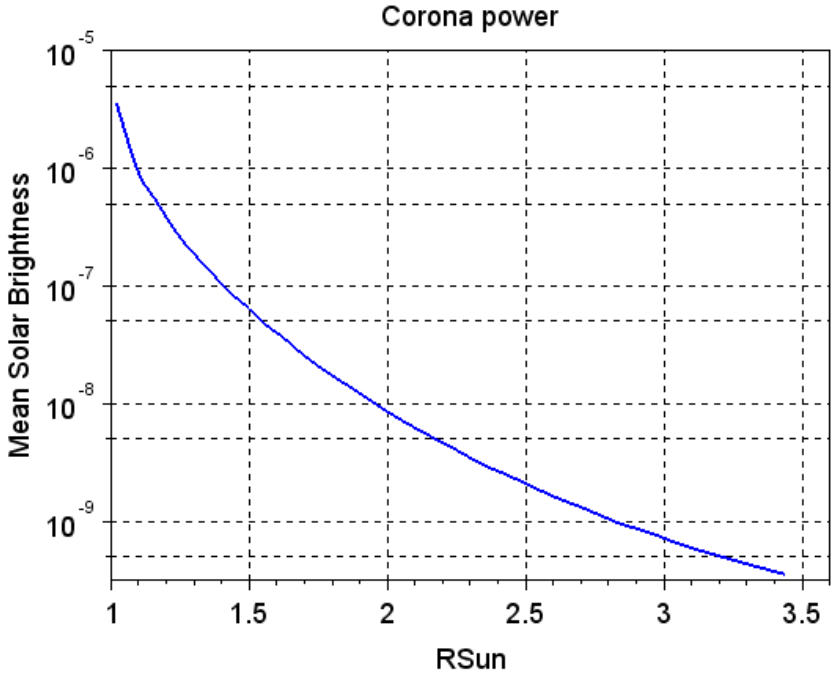

Figure 10 - K-Corona intensity angular distribution at entrance aperture (MSB)

2. GHOSTS AND SCATTERING: MODEL, ANALYSIS, PARAMETERS

2.1 Ghosts

As explained earlier, the contribution of each part of the corona to the straylight from multi-reflections on the detector shall be taken into account in order to get a realistic level of straylight. To illustrate this need, Figure 11 below shows the ghost distribution on the detector for a single FoV of 1.29RSun entering the instrument.

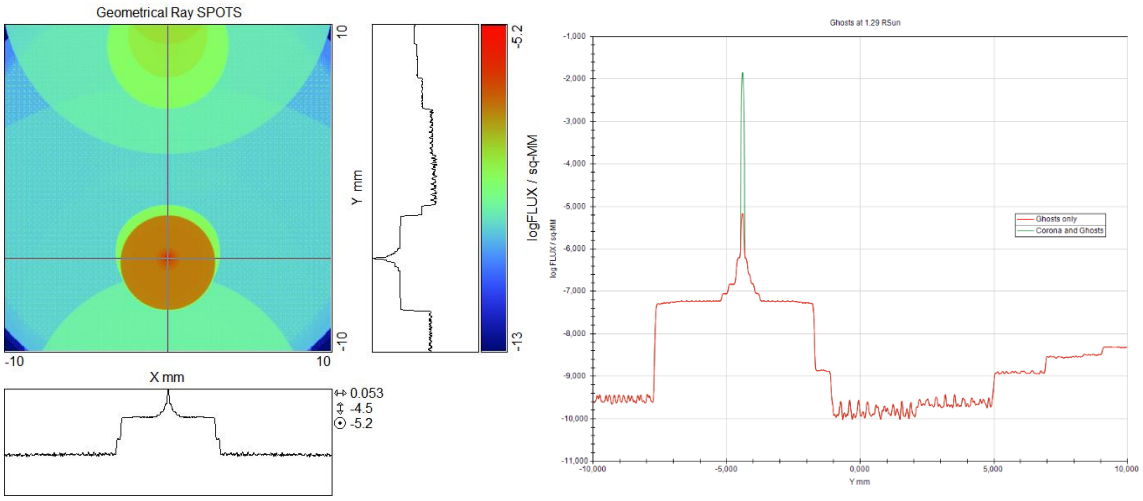

Figure 11. Ghosts distribution on the detector for a 1.29 RSun FoV (left) and transversal cut (right)

As seen on Figure 11 the ghost distribution is far from homogeneous on the detector. The spreading of certain ghosts (red curve) with respect to the location of the signal (green curve) indicates the need to compare each part of the detector ghosts to the signal that hits the detector in the same location.

In order to do that, it was decided to create a source with the same irradiance profile as the solar corona (actually several point sources along the FoV), and to propagate it altogether inside the instrument. Figure 12 below illustrates the propagation of the signal presented in Figure 10 above, without any multi reflections or scattering. This is the source that will be used to analyze the straylight due to the useful signal.

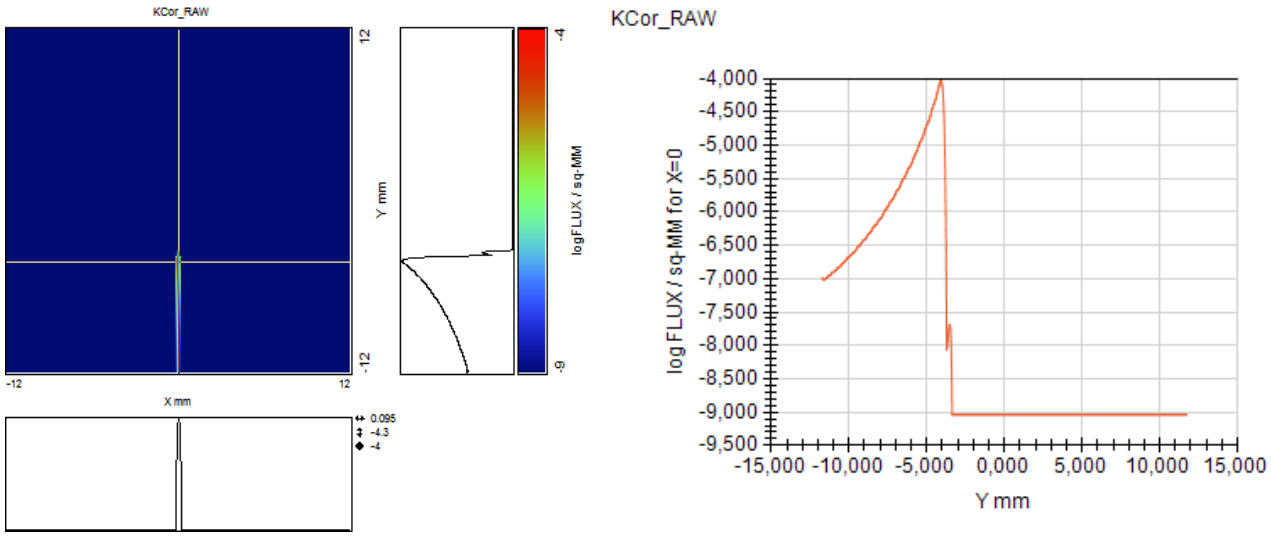

Figure 12. Propagation of the coronal signal inside ASPIICS without degradation

The image on the left shows the detector spatial irradiance of the coronal signal, and the curve on the right shows the profile cut.

The last operation to do to consider a realistic straylight level is to make a circular averaging in the end (can be performed as last operation as the instrument is circularly symmetrical with respect to the optical axis). That way the whole contribution of each part of the corona can be taken into account in each pixel.

Considering the model properties, following is the analysis steps and parameters:

1- Source points from 1.02 RSun (EO edge) to 4.30 RSun (maximum FoV in the corner) by steps of 0.02 RSun
   - The considered detector is slightly bigger than the real detector in order be able to create the source and still get the information up to 4.24 RSun on the Y or X axis
2- Each source point illuminates the entrance pupil with a circular grid of 201 rays (8021 rays total)
3- Each source point illuminates the pupil with the corresponding corona flux
4- Propagate the source inside the instrument with a chosen number of multi reflection and/or scattering
5- Get the total irradiance distribution on the detector
   - 2801x2801 10µm pixels, in order to take into account the 4.56RSun corner reported on the Y axis.
   - The considered detector is then around 28x28mm, but the real one is 20.5x20.5mm (2048x2048 10µm-pixels) (Figure 14)
6- Separate signal, ghosts and scattering
7- Apply circular symmetry with respect to the central pixel
8- Reduce to actual detector size

Figure 13 below shows the last steps of the analysis process. Steps 6 and 7 above were performed in another order in the figure, but this has no consequences on the results.

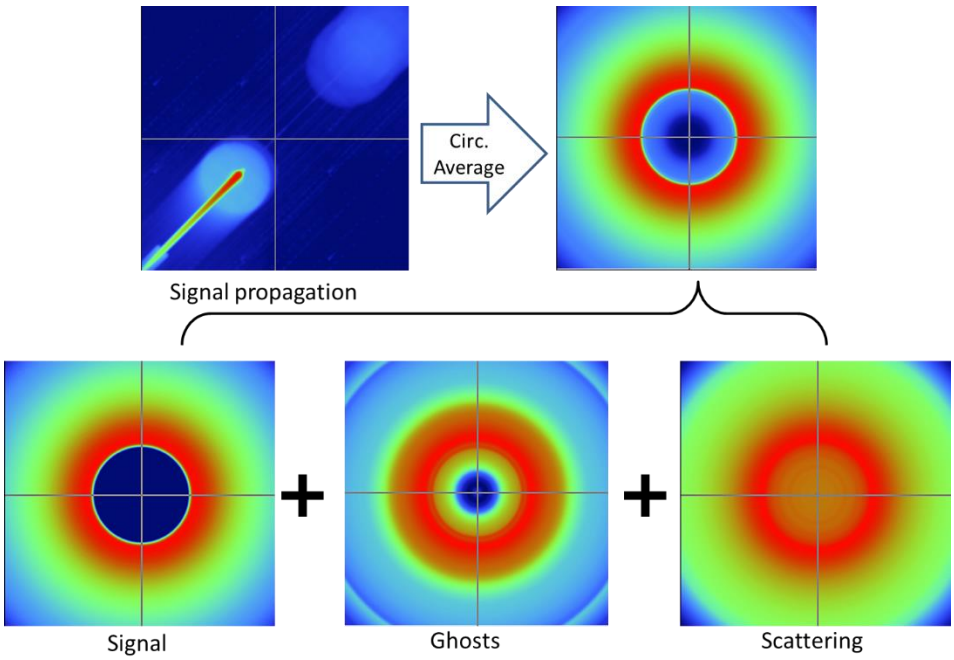

Figure 13. Illustration of the analysis process.

Figure 14 below shows the real detector limit on top of the analysis detector.

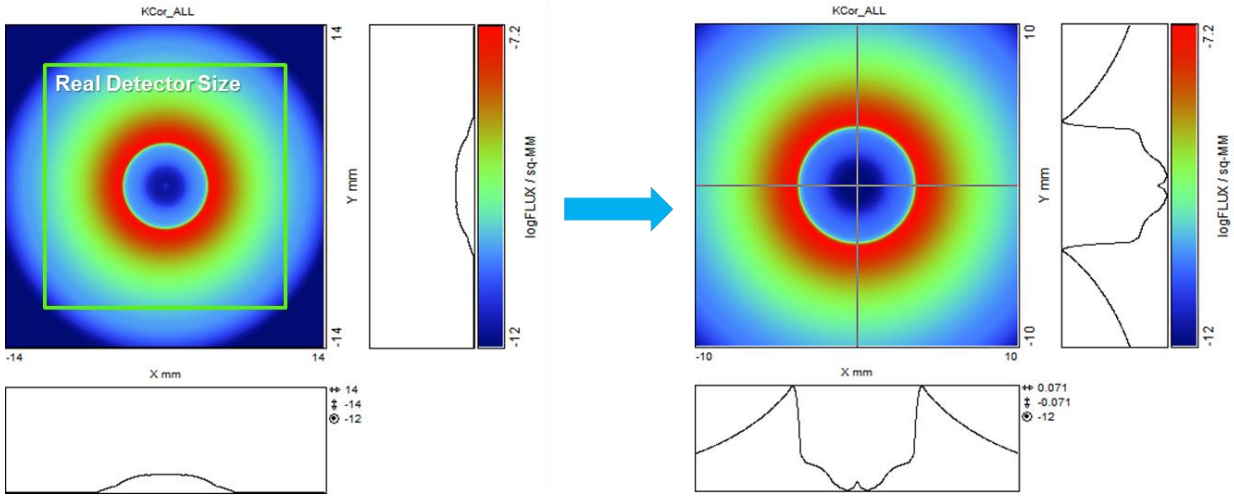

Figure 14. Coronal signal circular averaging, then crop to real detector size

The wavelength considered for the general analysis is **550nm.**

In order to take into account the slopes and the spectral band of the filters spectral transmission, an equivalent transmission was calculated to be used instead of the actual "peak" transmission at 550nm. This equivalent transmission is calculated to generate the same level of ghost at one wavelength than the real reflectance would do on the whole spectrum.

The equivalent transmission for the WBF is calculated at **95.2%** (instead of 99.8%). Figure 15 below shows the transmission curves as well as the calculated ghosts and the equivalent transmission for the wide band filter.

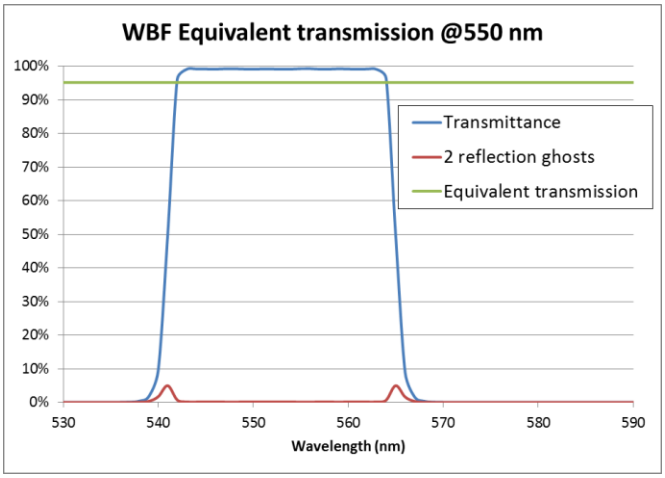

Figure 15. Equivalent transmission for the WBF

Concerning the detector, the reflectivity to take into account was decided and agreed with ESA as the measure showed a periodic pattern that could be different on the final detector. Figure 6 in §1.1 shows the measured detector reflectivity and the values considered for each operational spectral band, and specifically **15%** reflectivity for the [540-570]nm WBF filter.

Note: *This analysis only covers the White Band filter for now as no detailed transmission was provided for the narrow-band filters.*

The antireflection coatings that are presented in Figure 4 are used in the straylight model for each lenses or uncoated glass surface, except the front surface of the PO which is uncoated.

Concerning the primary objective, the back surface of the doublet is coated with a bandpass coating meant to cut down out-of-band light before even entering the instrument. This coating is designed by TOPTEC and will act together with the filters to guarantee no out-of-band light incident on the detector. Figure 16 below shows the predicted spectral transmission of the coating, based on measurements and 100 tolerances trials. At 550nm, the coating reflects **1.3%** of the incoming light.

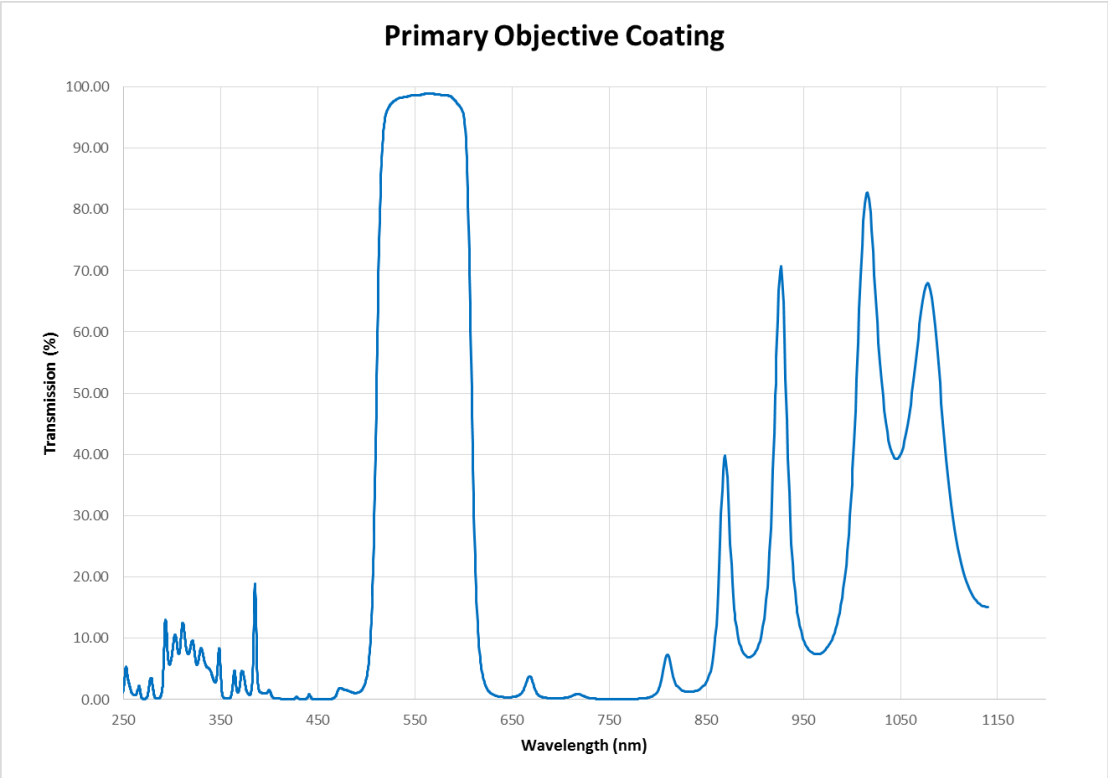

Figure 16. Primary Objective Coating transmission

Finally, the recent studies that led to the change of wide band filter also led to the consideration of adding a neutral density between the two most critical reflective surfaces of the design: the filters (5% - previously 12%) and the detector (15%). That way, the generated ghosts would be attenuated 3 times while the signal is only attenuated 1 time. The analysis was performed with several different locations for the Neutral density. The best location was found to be in place of the window in front of the detector. It was decided to put an absorbing neutral density of **50%,** so that the signal is attenuated by only 50%, while only 12.5% of the ghosts remain. This absorbing neutral density is located in place of the glass window in front of the detector.

2.2 Scattering

Due to the roughness of the optics (lenses, IO, window, filter) the light passing through these elements is scattered around the transmission direction. The amount of scattered light depends on the roughness amplitude. Possible roughness values are determined in function of the considered element and used in the following calculations to determine the possible amount and distribution of this stray light on the detector.

Several different scattering models are used in the literature to describe the scattering properties of a surface, depending on its micro-roughness. The best way to model accurately the scattering process is to measure the BSDF of each surface and fit the measurements with common models. However, it was not the case for the different lenses due to the amount of different glasses.

In order to get a good approximation of the scattering, the choice was then made to model scatter using the ABg model, which is available in most scattering software and used to approximate the scattering with good correlation in a lot of optical instruments before. This model and its interpretation are taken from [2].

This model is typically written:

$$BSDF(\beta - \beta_0) = \frac{A}{B + (\beta - \beta_0)^g} \ [sr^{-1}]$$

Where:

- $\beta = \sin(\theta_{scatter})$
- $\beta_0 = \sin(\theta_{specular})$

$A, B \ and \ g$ are the specific model parameters:

- $\frac{A}{B}$ equals the peak BSDF in the specular direction
- $B^{\frac{1}{g}}$ represents the angle at which the BSDF transition from a constant value to a power-law falloff
- g represents the slope, identical to the power-law falloff of the 2D PSD of the surface roughness

In order to be able to use this model, several assumptions need to be considered:

1- The surface roughness is considered isotropic
2- The considered surface roughness should be much less than the incident wavelength (for a wavelength of 550nm as it is the case here, the considered micro-roughness cannot be more than 1/100th, i.e. 5nm, which is easily met)
3- The spatial frequencies of the surface roughness are considered bounded by 1/D (surface diameter) and 1/λ

Observed on many optical surfaces, the parameters g (the slope) when measured is generally bounded between 1 and 2.5, and most commonly observed at 1.5. g=2.75 is occasionally observed on surfaces that could be defined as "super-polished"

In the same way, the transition angle $B^{\frac{1}{g}}$ is typically observed at 0.01 radians from specular. It is also postulated that this angle can be bounded between 0.01 and 0.0001 radians if the near specular measurement limitation prevents from measuring it.

However, the A and B parameters are not linked to something tangible. In order to make the connection, two other relations are needed.

The total integrated scatter (TIS) is approximated from the RMS roughness with the following equation (according to the Rayleigh-Rice theory, and being under the above-defined restrictions):

$$TIS = \left(\frac{2\pi . \Delta n . \sigma}{\lambda}\right)^2$$

Where σ is the RMS roughness, λ is the wavelength and Δn is the explicit refractive index difference.

Equating this expression to the usual TIS expression (usable for any scatter function, and which can be evaluated in closed form) lead to linking the surface roughness to the ABg parameters, allowing a good approximation of the surface scatter:

$$TIS = \iint BSDF(\theta, \varphi) . \sin(\theta) . \cos(\theta) \, d\theta d\varphi$$

The literature gives then simple expressions for A parameters given B and g assumptions:

Table 1. ABg parameters for lenses micro-roughness

g	B	A
2.5	0.00001	$0.35\left(\frac{\sigma\Delta n}{\lambda}\right)^2$
2	0.0001	$1.37\left(\frac{\sigma\Delta n}{\lambda}\right)^2$
1.5	**0.001**	$\mathbf{3.50}\left(\frac{\sigma\Delta n}{\lambda}\right)^2$
1	0.01	$6.35\left(\frac{\sigma\Delta n}{\lambda}\right)^2$

Given the assumption that for a conventional glass surface the slope g equals 1.5, and that the transition angle $B^{1/g}$ equals 0.01 radians, it was possible to run some tests to define an acceptable worst case. A quick evaluation confirmed that using the g=1.5 and B=0.001 line would lead to acceptable results of lenses scattering.

The DM lenses manufacturing brought some data about the real micro-roughness of each optical element. Taking some margins into account, we can reasonably estimate a worst case µroughness in order to take realistic hypothesis for the surface scattering. The real (measured) refraction index of the lenses was used in order to derive the A parameter for each surface.

The BSDF model corresponding to the DM measurements are considered as a worst case scenario for the scattering by the lenses. The specification being a bit stricter, a second case of scattering was analyzed, which corresponds to what was specified to TOPTEC. Concerning the realistic values of µroughness, what was achieved for the DM lenses is considered by TOPTEC as the best they can achieve.

The considered roughness values as well as the corresponding TIS and A parameter are summarized in Table 2 below.

Table 2. Considered roughness, TIS and A parameter on each optical element

Element	Meas. σ_{RMS} (nm)	Model σ_{RMS} (nm)	TIS	A Param.	Element	Meas. σ_{RMS} (nm)	Model σ_{RMS} (nm)	TIS	A Param.
PO-L1 S1	0.6	1.0	0.0035%	3.1e-6	**O3-L2 S2**	1.9	2.0	0.0344%	3.1e-5
PO-L1 S2	0.6	1.0	0.0035%	3.1e-6	**O3-L3 S1**	1.6	2.0	0.0261%	2.3e-5
PO-L2 S1	0.6	1.0	0.0063%	5.6e-6	**O3-L3 S2**	0.6	1.0	0.0065%	5.8e-6
PO-L2 S2	0.7	1.0	0.0063%	5.6e-6	**O3-L4 S1**	1.6	2.0	0.0302%	2.7e-5
O2 S1	0.8	1.0	0.0086%	7.6e-6	**O3-L4 S2**	1.8	2.0	0.0302%	2.7e-5
O2 S2	2.6	3.0	0.0773%	6.9e-5	**O3-L5 S1**	1.1	2.0	0.0261%	2.3e-5
O3-L1 S1	2.5	3.0	0.0455%	4.0e-5	**O3-L5 S2**	1.4	2.0	0.0261%	2.3e-5
O3-L1 S2	1.7	2.0	0.0202%	1.8e-5	**Filters**	N/A	1	0.0035%	3.1e-6
O3-L2 S1	3.0	3.0	0.0773%	6.9e-5	**Window**	N/A	1	0.0035%	3.1e-6

Figure 17 below show the BSDF curves corresponding to each surfaces for a 0° incidence angle, corresponding to the measured µroughness of the DM lenses.

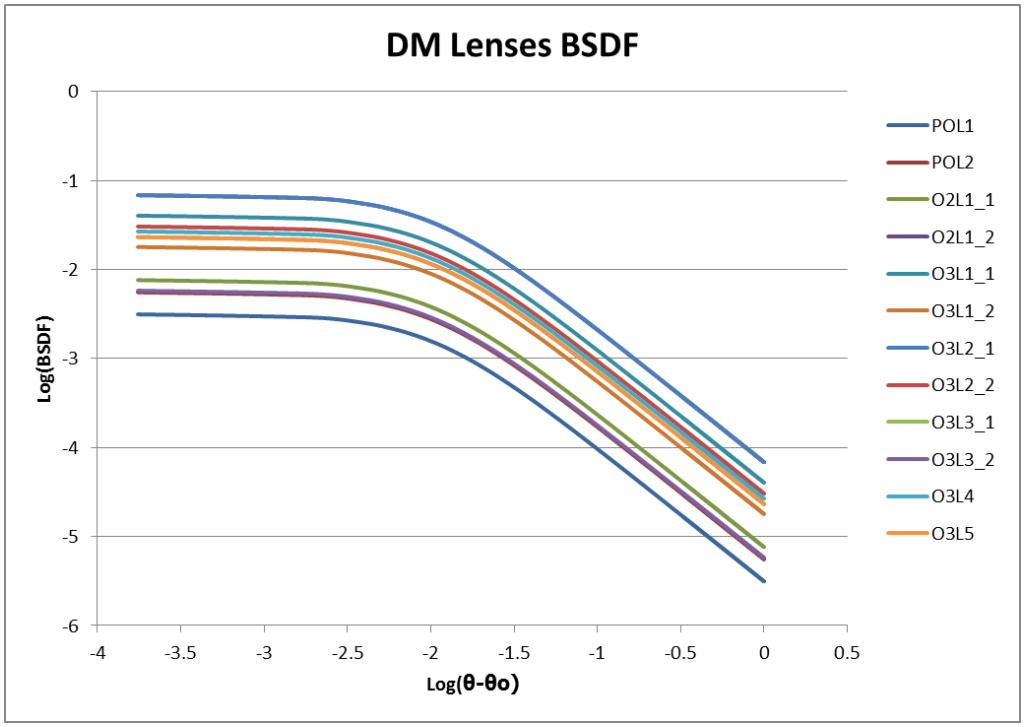

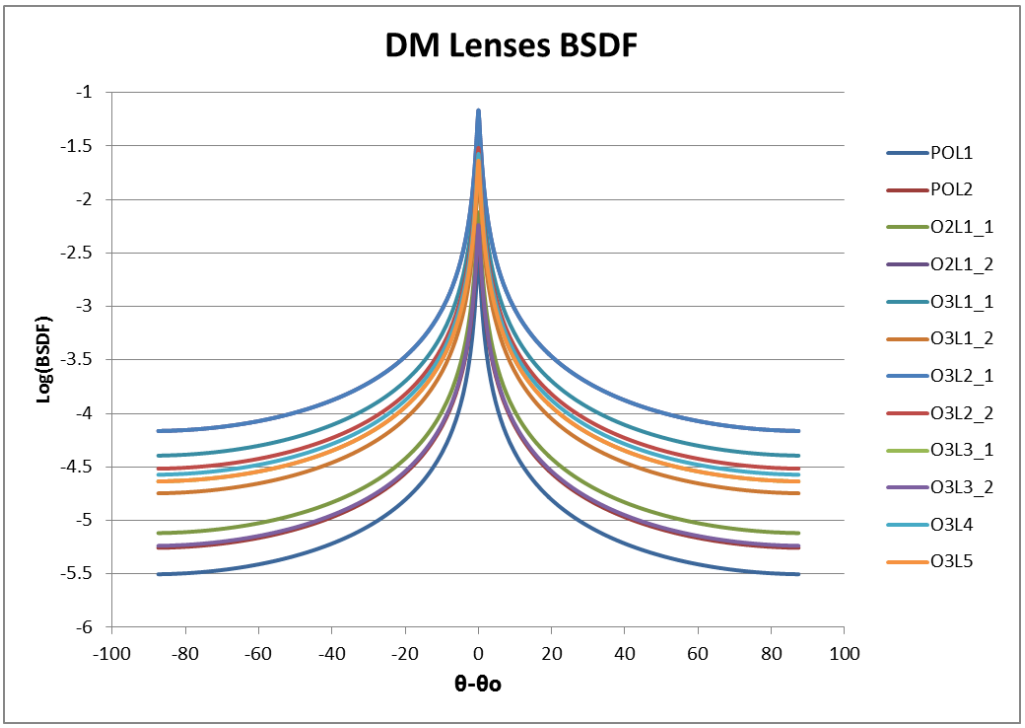

Figure 17. DM lenses log(BSDF) versus log(angle) (Up) and Log(BSDF) versus angle (down)

3. IN-FOV STRAYLIGHT

3.1 Source: solar corona

As seen earlier, the best way found to simulate the In-FoV straylight (generated by the corona) was to propagate one complete radius of the K-Corona inside the instrument, and calculate for this complex source the associated ghosts and scattering that will reach the detector. This has been performed for the roughness case presented in §2.2. The DM roughness case is what was achieved during the DM model manufacturing of the lenses.

The analysis made considering the DM roughness case led to the following results.

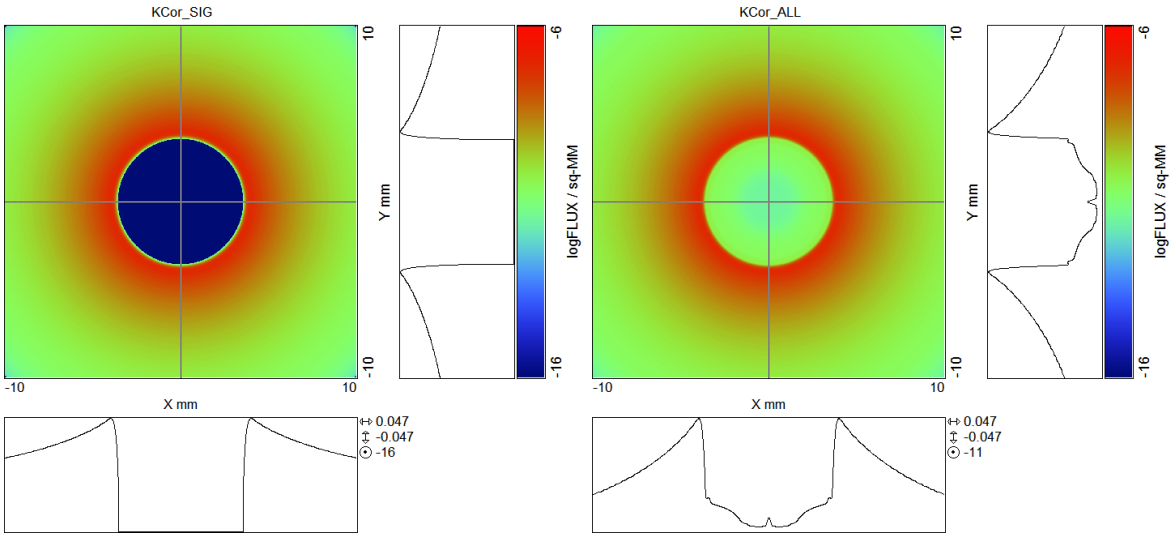

Figure 18. Signal (left) and Total detector irradiance (Right)

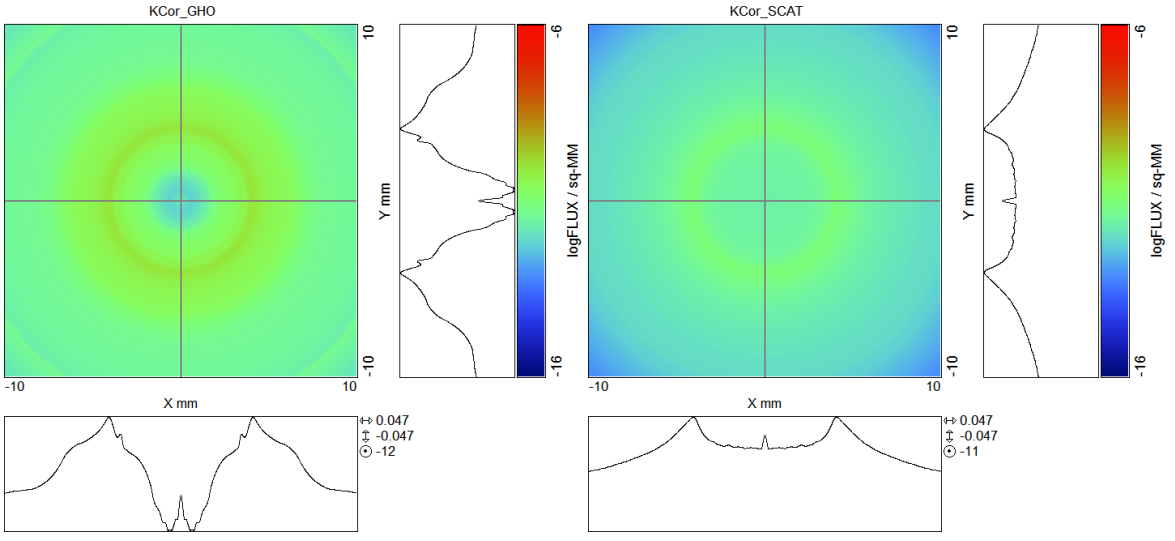

Figure 19. Ghosts (left) and Scattering detector irradiance (Right)

Figure 18and Figure 19 above represent the irradiance on the real detector size (10.24x10.24mm) considering ghosts, scattering and signal separately. The color scale is the same for the four pictures, giving a first idea of the straylight level associated with each case. Following the description of §2, the analysis was performed on a larger detector to account for straylight created by the whole FoV.

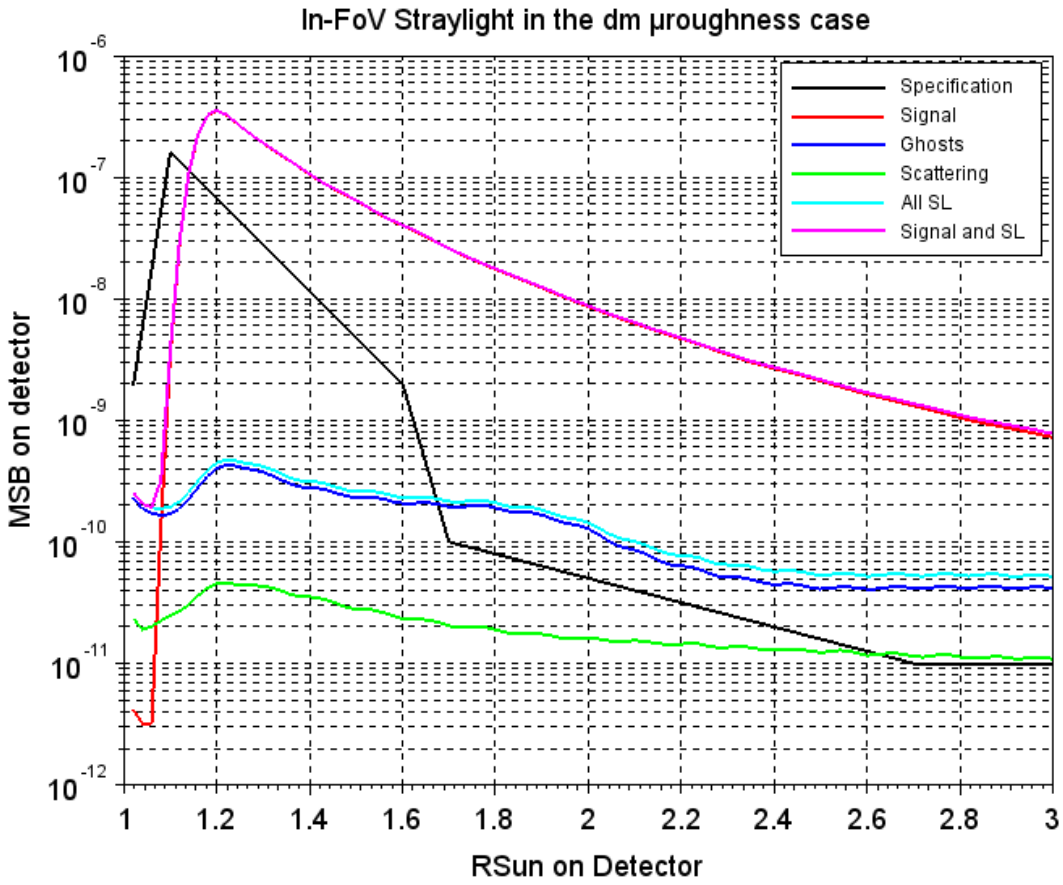

Figure 20. In-FoV Straylight Level in MSB

Figure 20 above shows the comparison between the specification and all the irradiances concerned by the straylight analysis. For the first figure above, the irradiance is expressed in MSB (mean solar brightness) per pixel, the corona radius source having been entered in MSB as well. In order to account for the error made by circularly averaging, a unitary flux radius was sent using the same exact parameters and transformations.

Dividing the resulting corona and straylight irradiance by the unitary irradiance result allowed retrieving the final irradiance in MSB on the detector.

As we can see on the curves, the straylight due to the scattering on the lenses is already a bit over the specification after 2.6 RSun. Concerning the ghosts, this is already the case after 1.7 RSun. The reason for this specification outreaching is that the corona has a very high dynamic range (there is a factor of 1000 between the corona intensity around 1 RSun and 3 RSun). Considering this dynamic range, having a detector reflectivity of around 15% is a huge aggraving factor and nothing can completely discard this impact.

The filters reflectivity was already optimized by changing the supplier, and a neutral density was added in the path in order to reduce the ghosts. As we can see, this is not enough to be under the specification, but the result is still satisfying after discussions with the scientific team.

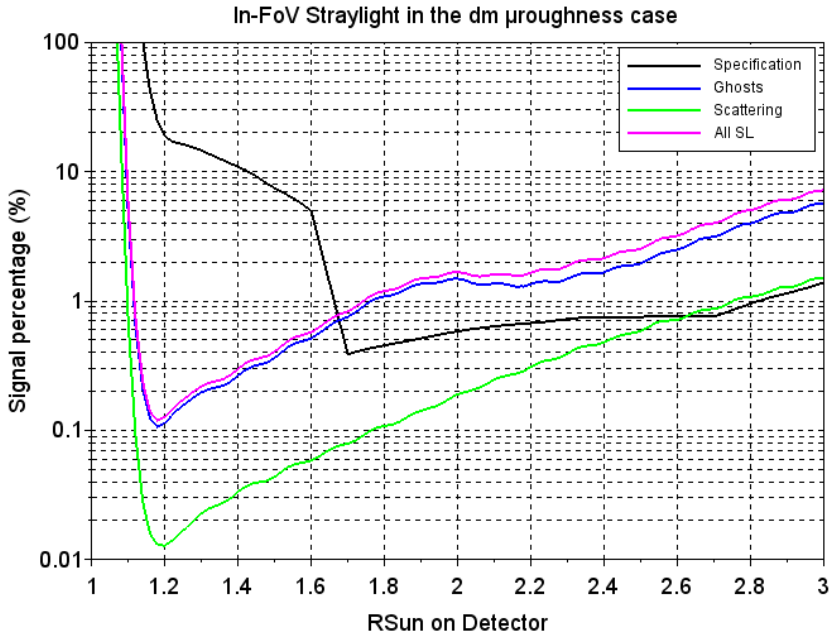

Figure 21. In-FoV straylight, expressed in corona signal percentage

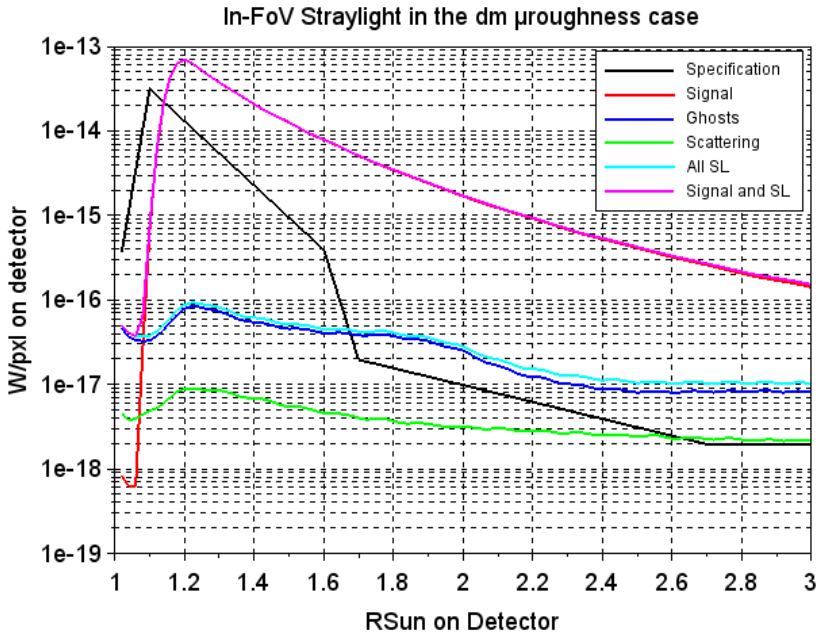

Figure 22. In-FoV straylight expressed in W/pxl

Figure 21 and Figure 22 above represent the same comparison with different units and scales. The first one expresses the straylight level in terms of signal percentage, while the second one uses the sun irradiance of aproximately 1.10^{-7} W/pixels to represent the straylight level in W/pxl.

The sun irradiance was calculated, taking into account 54W/m^2 at the entrance pupil, the area of the sun image on the detector (disk of 341 pixels radius), and an approximate ASPIICS instrument transmission of 33.75% (taking into account the 50% neutral density)

3.2 Source: Occulter Position Sensor Emitter (OPSE)

The OPSE is a subsystem located on the Occulter Spacecraft, facing the entrance of the ASPIICS instrument. It is composed of three different LEDs, located on a 200mm radius circle around the occulter center. The signal of these LEDs is meant to be read on the same detector that will observe the corona signal. To this aim, the internal occulter is designed with a hole.

This hole allows the OPSE signal reaching the detector, but then also creates unwanted reflections and scattering on the lenses surface. It is then mandatory to observe that and compare it to the Corona signal, in order to verify that the straylight caused by the OPSE will not pollute the observations.

To simplify the simulation, and as no particular location was decided at the time for the OPSE around the EO center, a uniform placement was simulated (3 source points, each located at 120° around the 400mm diameter circle of the EO center).

The flux of each led in the entrance pupil is given in the LEDs datasheet to be of 0.15mW (typically) for an emission angle of ± 6°. Considering an entrance pupil of 25mm radius located at a distance (ISD) of 144,348m, one OPSE LED was calculated to generate an irradiance of **$2.1x10^{-7}$ W/m^2** at the pupil plane. The sun radiance in the pupil plane considering the only white light filter and the PO filter passband is **54.2W/m^2.**

Knowing all that, the OPSE irradiance in the pupil plane was calculated to be **3.8×10^{-9} MSB** (mean solar brightness).

The source points were then simulated to illuminate the entrance pupil of ASPIICS with a **3.8×10^{-9} W** flux. As the Solar corona is also simulated with a flux in the entrance pupil in MSB, the result of the simulation for the OPSE will directly be comparable to the solar corona signal.

Figure 23 below presents the K-Corona signal on the detector and the combination with the OPSE signal and straylight (ghosts + scattering). Figure 24 below show the decomposition of the straylight from the OPSE with the same color scale as the previous figure. Lastly, Figure 25 presents the In-FoV signal and straylight, combined with the OPSE signal and straylight as irradiance on the detector plane. The color scale was adapted to get a better rendering.

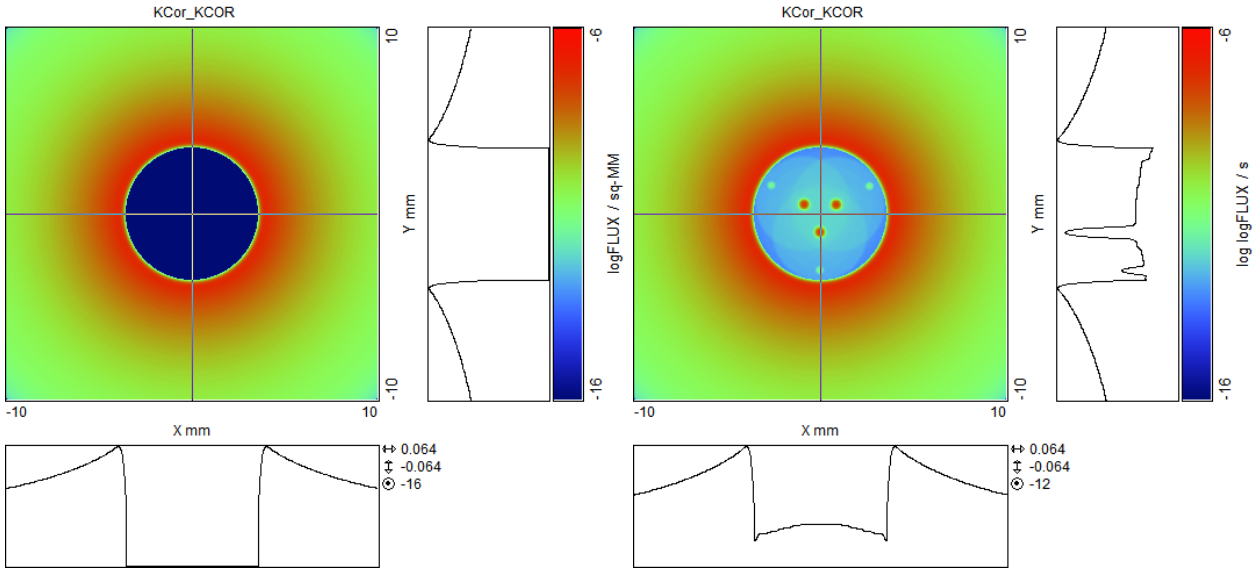

Figure 23. K-Corona signal (left) and combination with OPSE signal (right)

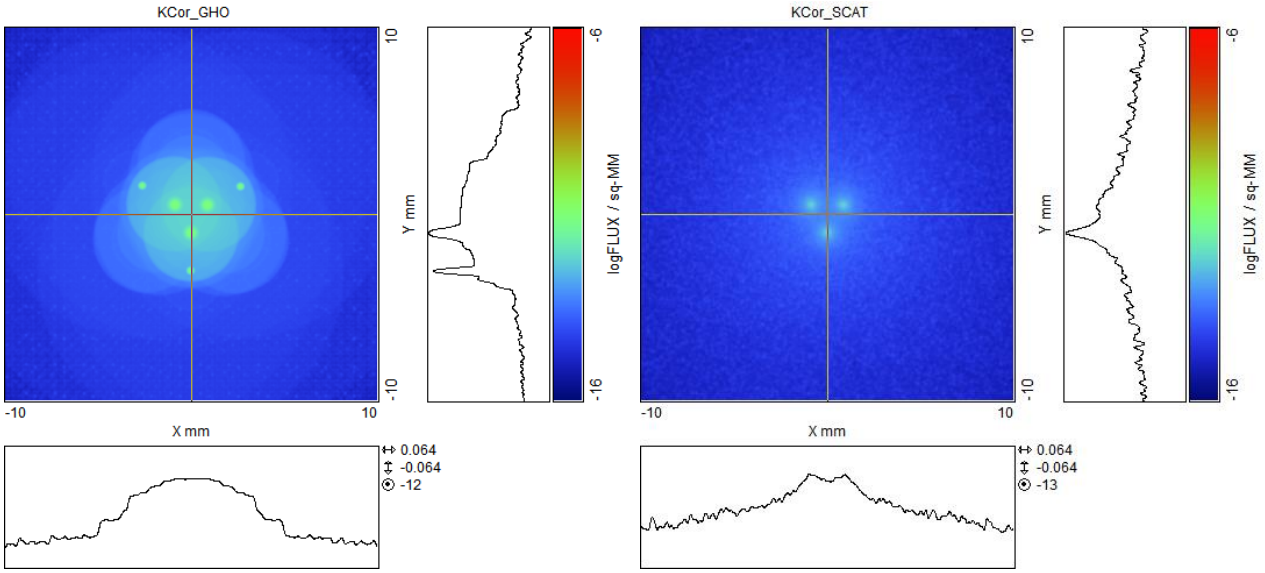

Figure 24. OPSE ghosts (left) and scattering (right) irradiance on the detector

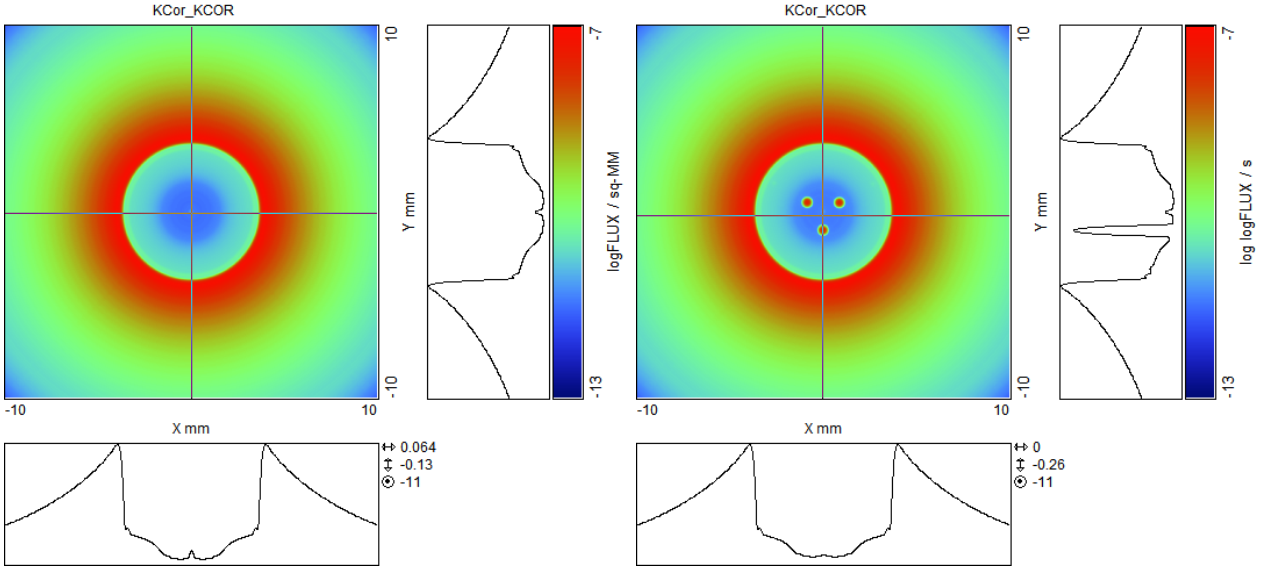

Figure 25. In-FoV Straylight and signal (Left), and combined with OPSE straylight and signal (right)

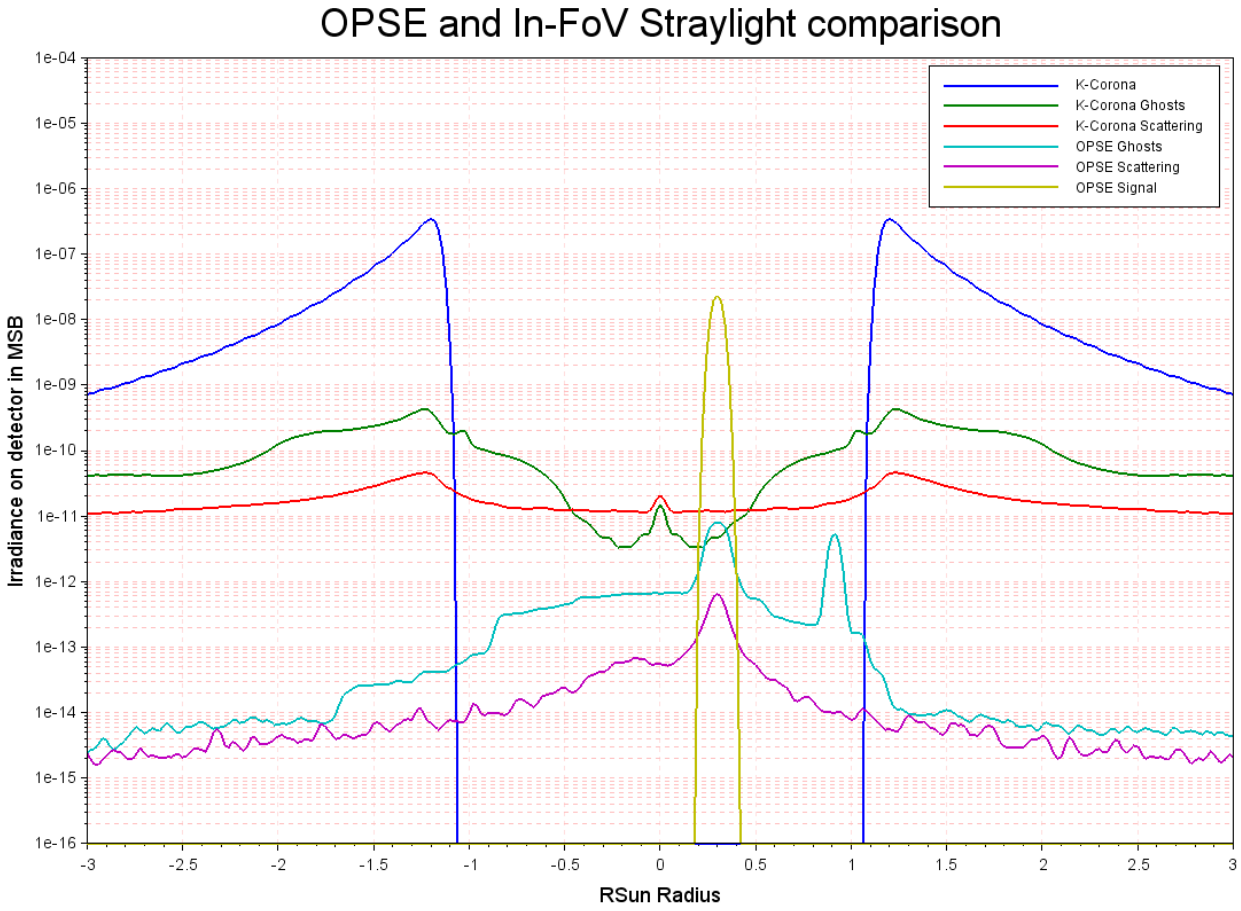

Figure 26. Comparison with In-FoV Straylight

Figure 26 above shows the comparison of the OPSE signal and straylight irradiance distribution on the detector with that of the previously presented In-FoV Straylight. As we can see, the K-Corona straylight is around 1000 times lower that the OPSE signal.

At 0.3 RSun which is the OPSE signal peak irradiance:

1- The OPSE irradiance is 2.35 x 10-8 MSB/pxl

2- The all-combined Straylight irradiance is 2.5 x 10-11 MSB/pxl

However, the straylight produced by the OPSE that could reach the part of the detector dedicated to the corona observation is really low compared to the straylight induced by the K-Corona itself (between 1 and 3 RSun). The impact of the OPSE straylight on the K-Corona observation is then considered inexistent.

4. IN-FOV STRAYLIGHT SOURCE: EXTERNAL OCCULTER DIFFRACTION

The diffraction of the sun rays by the external occulter took some time to be correctly estimated.

For starter, the created irradiance in the entrance pupil cannot be simulated by ASAP™ due to the fact that it uses ray-tracing features. Diffraction can be modeled to some extent considering a Gaussian beams decomposition of the electromagnetic wave. It implies defining Gaussian beams with several geometric rays, which will carry different properties such as the propagation direction, the divergence of the beam, and its waist.

Compared to a simple geometrical optic ray tracing calculation, the number of ray needed to simulate diffraction is generally 4 times higher (up to 8 depending on the system). Also, due to the divergence of the beams, long propagation distances are not possible without resampling the wavefront, which add calculation time. The distance between the EO and the entrance pupil is already quite large and several resampling (decompositions) would be needed. Lastly, seeing that what is needed is already a really small portion of the diffraction pattern produced by the EO edges, a pretty high number of rays would be needed to get the right diffraction profile on the entrance pupil (entrance pupil diameter is more than 28 smaller than the EO diameter).

The combination of all these reasons makes the EO diffraction simulation really complicated to perform (too much time & memory consuming) with a ray-tracing software like ASAP™.

For the ASPIICS straylight analysis, the diffraction profile from the sun hitting the External occulter was calculated externally by INAF, with another software (VirtualLab™) using physical optics calculation rather than only ray-tracing. They were able to simulate the External occulter diffraction and provide us with the diffraction profile at the entrance aperture of ASPIICS. For more information on the EO diffraction simulation and its verification, see [7] (Diffraction calculation) and [8] (Diffraction simulation verification by a scaled-model). Figure 27 below shows the complete diffraction irradiance for one radius on the pupil plane.

The provided diffraction profile is normalized with respect to the Sun irradiance in the pupil.

The diffraction plays a role in the umbra/penumbra intensity up to a distance of about 130cm from the center of the pupil. Concerning its impact on the amount of straylight entering the instrument, only the part before 2.5cm is of interest as the pupil is only 5cm in diameter. The diffraction profile from 0 to 2.5cm was then used to create an apodization of the source in the pupil plane, what will be used to propagate the diffraction inside the instrument. Figure 28 below shows the apodization function created. The profile for the diffraction by a torus edge was used.

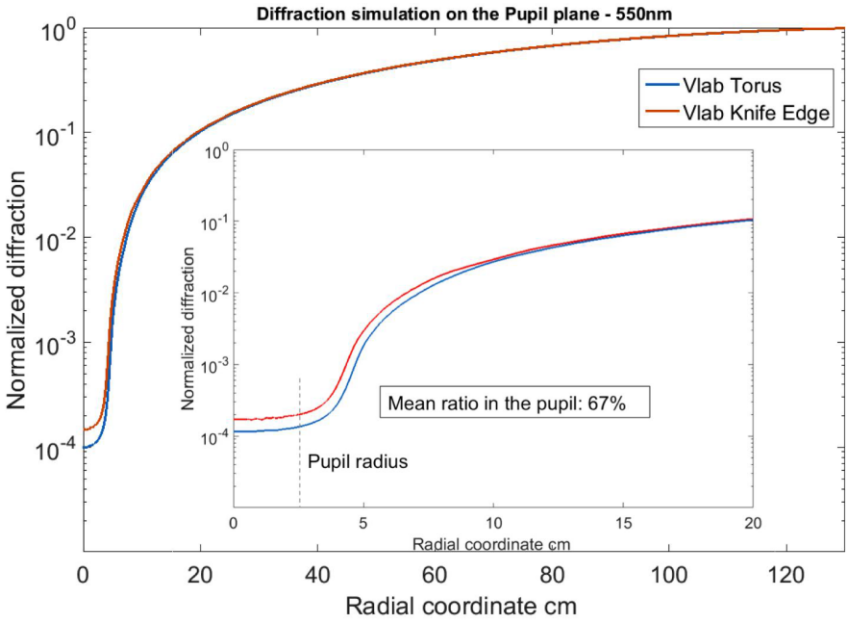

Figure 27. Diffraction profile on the pupil plane for two different EO shape

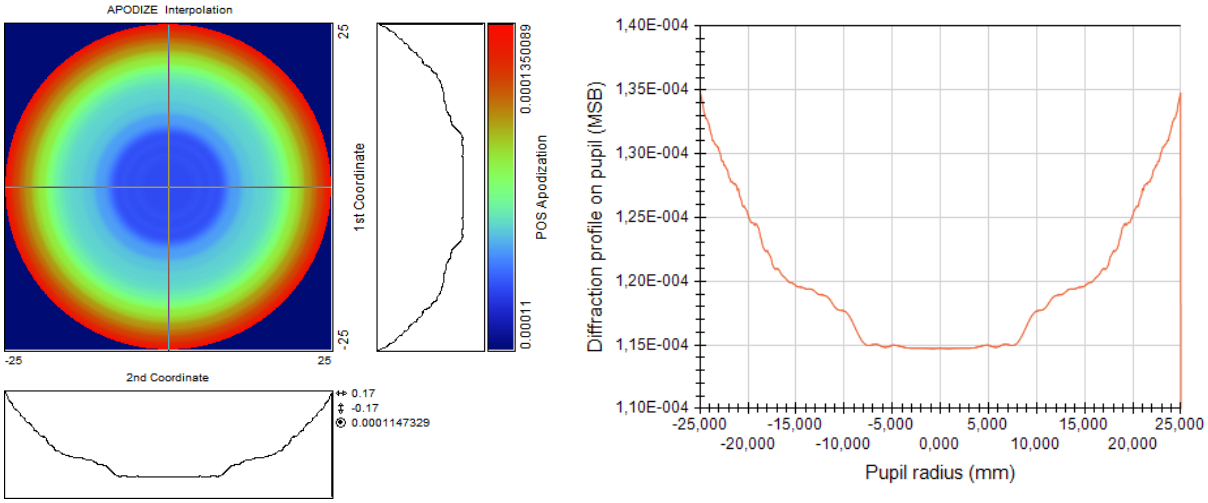

Figure 28. Pupil apodisation with diffraction profile

The torus-like shape of External Occulter was the considered case for this analysis.

First idea : ring of source

In order to propagate the diffraction, the first idea was to create a ring of source point on the edge of the external occulter (144348m away from the pupil, 1420mm diameter). After several tries, a source with the following properties was created:

- 360 source points uniformly placed around the edge of the internal occulter.
- Each one of this source point illuminates the entrance pupil with an elliptical grid of 51 x 51 rays
- The combination of the irradiance of all the point source is apodized by the diffraction profile from Figure 27 above

This created source is then propagated inside the whole instrument, and allowed to:

- Reflect 4 times (SPLIT 4)
- And/or scatter 1 time

Scattering one time more was tested on a smaller number of rays, but the second scattering did not bring more relevant straylight while making the simulation impossible to complete in a reasonable amount of time due to the amount of rays created.

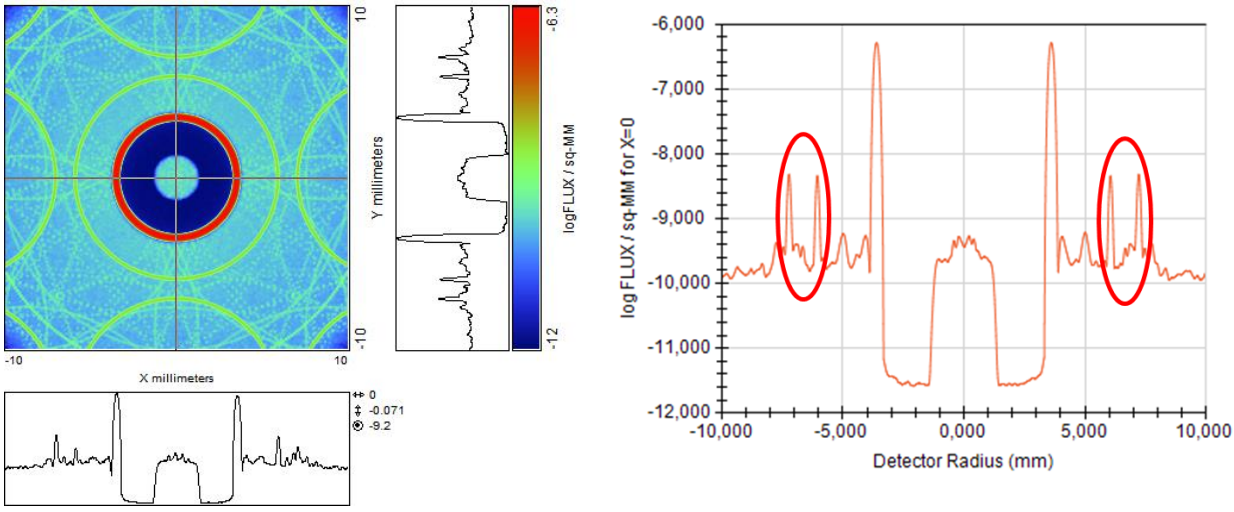

Figure 29. Ghosts and scattering from a ring on EO edge

After propagation, reflection and scattering on the lenses surfaces, the resulting irradiance on the detector is presented on Figure 29 above. The first thing to notice is that is created ring-shaped patterns that are probably due to the ring of point source. A careful separation of all the created ghosts allowed isolating one in particular that seemed to have a high intensity. This is the one circled in red on the figure.

This ghost was created by the reflection between the front ant the back surface of the primary objective (PO).

These two surfaces are known to create a ghost that spreads onto the whole detector with a not to high intensity. The reason why it creates here a pretty high intensity ghost is because of the sampling of the source. As the ghost is highly spread, it means that it needs a high number of rays on the pupil to be correctly represented on the detector.

The source was then created again, this time with 501x501 rays inside the pupil. Only the surfaces of the PO were allowed to reflect rays. The resulting irradiance pattern on the detector is shown on Figure 30 below. After averaging, the ghosts from the PO (green) is spread as expected, and has a much lower intensity than before.

Launching a ring of 360 source points on the PO edge, each of them illuminating the pupil by a circular grid of 501x501 rays would prove to be impossible to simulate due to the high number of surfaces, and the high number of child rays that ghosts and scattering would need to get a representative straylight irradiance pattern on the detector. Another way to simulate this needed to be used.

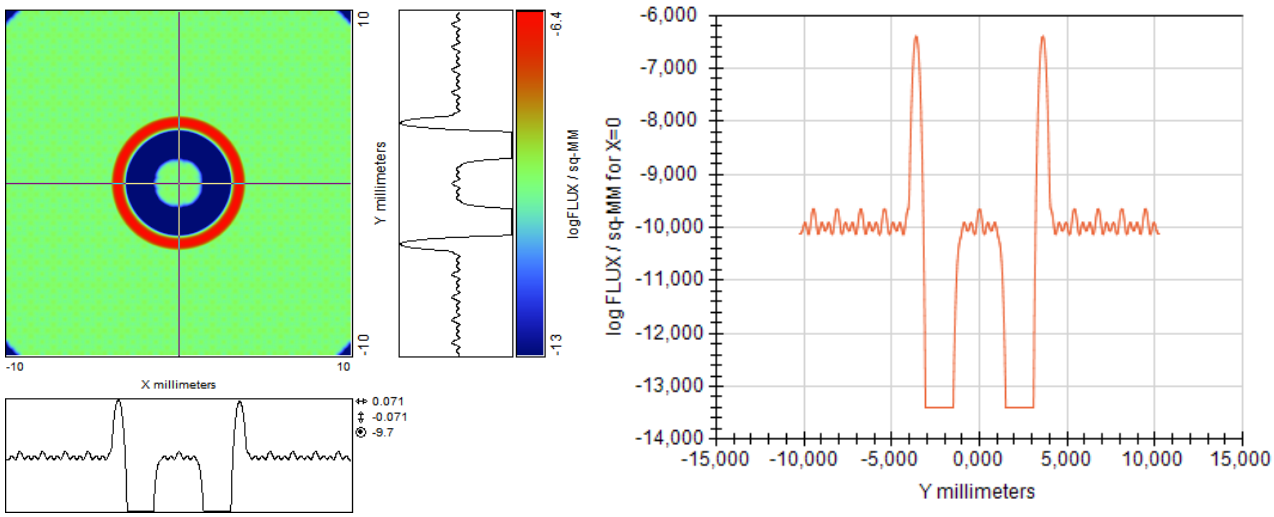

Figure 30. Ring of sources, ghosts from PO only, 501 rays on pupil grid

Final way: only one point on the EO edge

The idea is that the system being circularly symmetric, the irradiance corresponding to the ring of point source could be retrieved by making a circular average of the irradiance on the detector for 1 only source point.

As verification that the two ways would both give a representative final irradiance, the same simulation of PO ghosts straylight was launched for both sources definition.

Figure 31 below shows the resulting irradiance pattern for the ghosts created by the primary objective only. After circularly averaging, the comparison of the irradiance distribution with the one from Figure 30 above brought enough confidence about the similarity of the two simulations. The peak maximum ($4.77.10^{-7}$ and $4.76.10^{-7}$ W/mm²) corresponded. The average of the ghost level ($1.213.10^{-10}$ and $1.206.10^{-10}$W/mm²) also corresponded with enough accuracy.

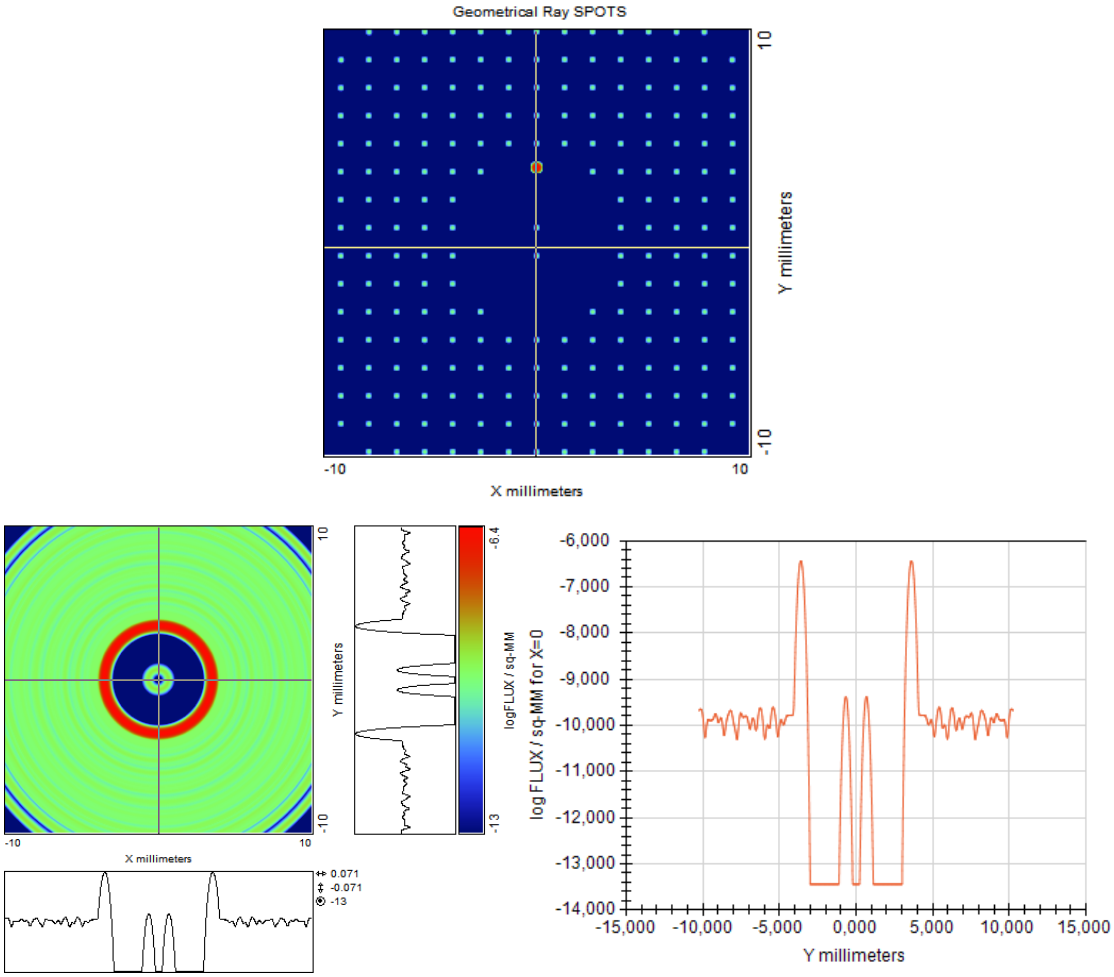

Figure 31. Only one source point, ghosts from PO only, 501 rays, before (up) and after (down) circular averaging

After verification, the final EO diffraction straylight computation could be set.

In order to be sure to get the right distribution of irradiance for each ghost, a high number of rays needed to be defined in the pupil grid. 501 x 501 rays was found to be a good sampling. This time then, only one source point was defined on the edge of the EO:

- 1 source points at the edge of the external occulter
- Illuminates the entrance pupil with an elliptical grid of 501 x 501 rays
- Irradiance at the pupil is apodized by the diffraction profile from Figure 28 above

This created source is then propagated inside the whole instrument, and allowed to:

- Reflect 4 times (SPLIT 4) (2^{nd} order ghost)
- And/or scatter 1 time (1^{st} order scattering)

It should be noted that the pupil grid cannot not be defined with more rays due to ASAP internal limitation for spatial apodization.

Figure 32 below shows the decomposition of the final straylight irradiance pattern into a ghost-only irradiance, and a scattering-only one. The color bar is adapted for each picture, but it is quite easy to see on the left picture that the scattering impact is mostly uniform already before averaging.

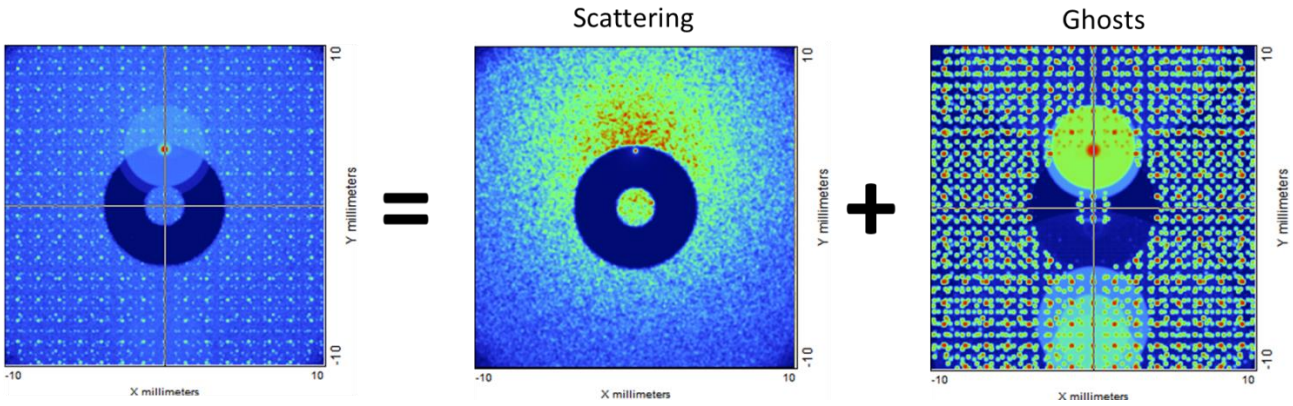

Figure 32. Ghosts and scattering from one source point on EO edge – 501x501 rays in pupil

In order to get a realistic straylight irradiance distribution, a circular averaging is then made so that it simulates the irradiance distribution from the whole circular edge of the EO rather than only one source point. This circular averaging is shown on Figure 33 below.

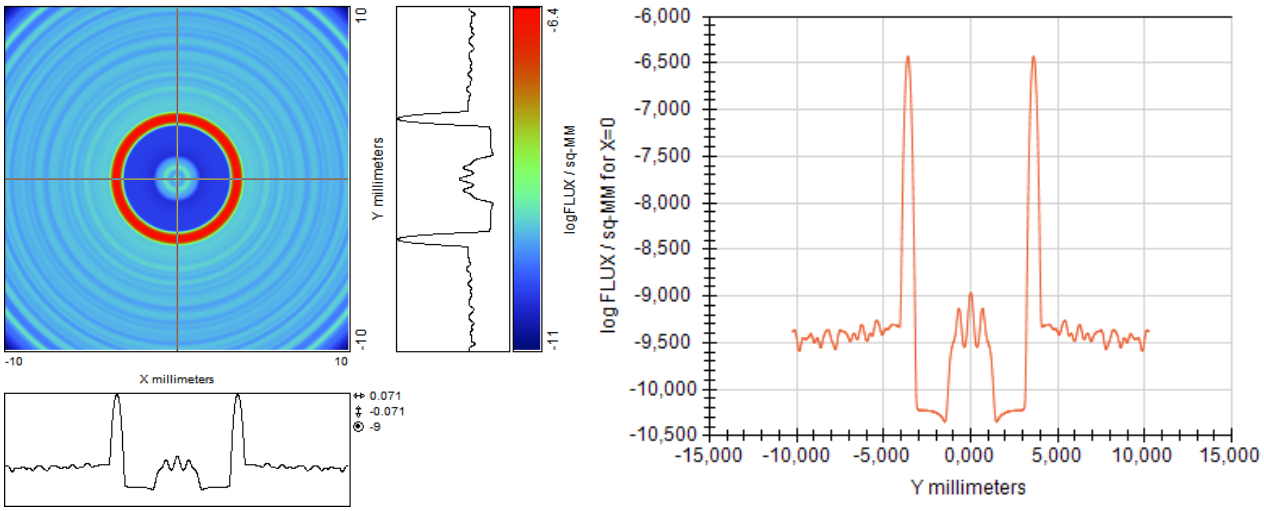

Figure 33. Final EO diffraction straylight irradiance on the detector after circular averaging

In order to compare the irradiance distribution on the pupil plane to the specification, we need to first compare the irradiance on the detector to that of the full sun. As the apodization was already relative to the sun brightness, the idea is to propagate the full sun inside the instrument, with a unitary apodization inside the pupil.

The internal occulter was removed in order to propagate the whole sun onto the detector. The created source had the following properties:

- 51 x 51 rays in an angular grid defining the collimated sources direction
- 51 x 51 rays in a spatial grid at the pupil level defining the pupil illumination by each of these sources.
- The combined irradiance of all the source points is then apodized by a unitary function, shown in Figure 34 below.

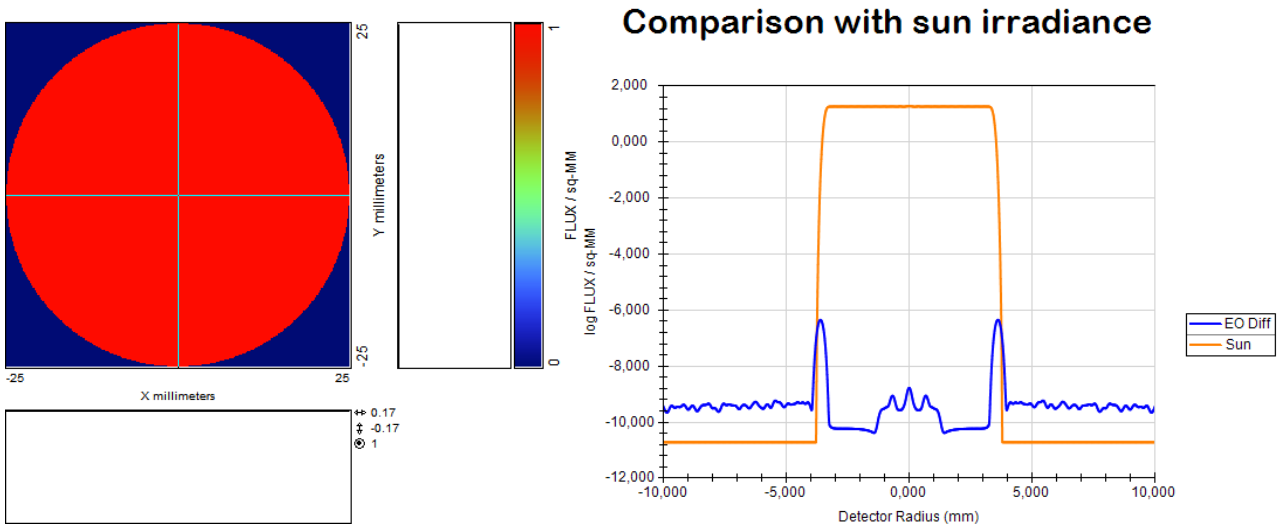

Figure 34. Sun source irradiance on pupil plane (left) and comparison on the detector plane (right)

The straylight specification being then express in terms of mean solar brightness, the EO diffraction irradiance was normalized with respect to the sun average irradiance, and then compared to the KCorona signal and straylight irradiance that was calculated and simulated in §1.4 and §3 above.

Figure 35 below shows that final comparison. It must be noted that the diffraction peak around 1RSun is due the residual transmission of the internal occulter (around 10^{-4} for the moment). The internal occulter real characteristic is not yet defined, and it is highly possible to decrease even more the residual transmission, only by thickening one layer of the coating.

The diffraction intensity begins to be under the (vignetted) corona after 1.104 RSun. The diffraction is less than 1% of the corona after 1.133 RSun. The internal occulter having a diameter of 1.79mm, the corona is 50% vignetted at 1.164RSun and is not vignetted anymore at 1.201RSun.

In this configuration, the diffraction straylight irradiance stays under the specification.

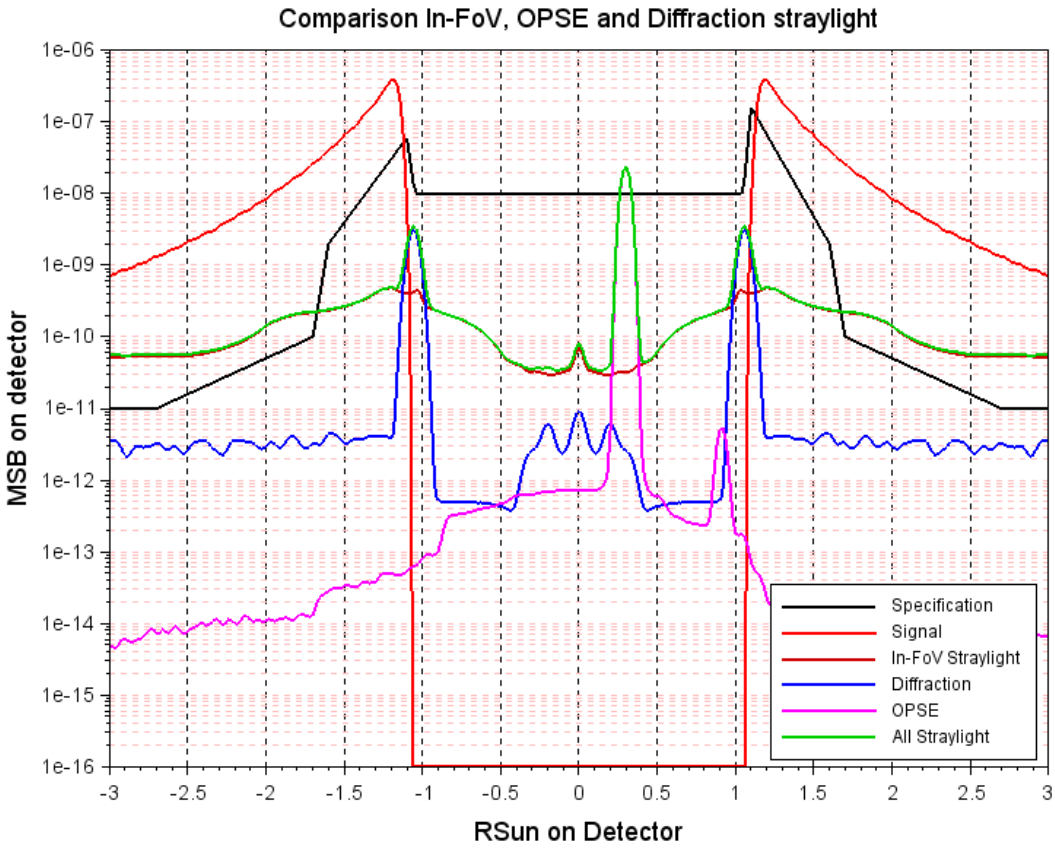

Figure 35. Final comparison of EO diffraction straylight with the KCorona, the in-FoV straylight and the specification

As seen on Figure 35 above, the main diffraction straylight path occurs at the same location than its direct image on the detector plane. This is mainly due to the fact that the internal occulter has a residual transmission. This residual transmission can easily be cut down by thickening the absorbing layer. Once the internal occulter will be manufactured, this residual transmission can be adjusted to reduce the intensity of this straylight contributor. Concerning the ghosts, the main ones are created by multireflections between the internal occulter and the PO surfaces. However, all those ghosts are spread out onto the whole detector and add up to the diffraction part that is scattered by the lenses.

The diffraction by the external occulter which could then be diffracted again onto the pupil's edge will be strongly cut down by the Lyot Stop, and this straylight contributor quite obviously would be lower than the straylight coming from the direct diffraction on the EO edge.

The propagation of the diffraction itself through the ASPIICS instrument was not performed at this time, but the diffraction signal itself should be added to this comparison to get a full overview of the in-FoV straylight. This calculation is being made through a numerical model presented in [9] and [11].

5. CONCLUSION

This paper presented the last results of the in-FoV straylight analysis for the ASPIICS coronagraph. The key point being that analysis showed that the initial specification did not fully represent the complexity of the observation and cannot be reached. A number of adjustments were made (better filters, add of a neutral density) to decrease the straylight irradiance down to an acceptable level.

Following this analysis, some hypotheses and parameters can be refined to better fit with the reality:

1- To consider real BTDF measurement of lenses in the μroughness scattering model

2- To consider a contamination model (following Mie theory) that will add to the μroughness scattering

3- To add the propagation of the diffraction as calculated in [9] to the final straylight irradiance

4- To consider a way to use the real diffraction profile and compute the generated straylight

ACKNOLEDGEMENTS

The ASPIICS project is developed under the ESA's General Support Technology Programme (GSTP) and the ESA's Prodex Programme thanks to the sponsorships of seven member states: Belgium, Poland, Romania, Italy, Ireland, Greece, and the Czech Republic.

ESA Director of Science and Robotic Exploration has appointed Dr Andrei Zhukov of the Royal Observatory of Belgium as Principal Investigator for the ASPIICS instrument.

REFERENCES

[1] Lamy, P., Vives, S., Damé, L., Koutchmy, S., "New perspectives in solar coronagraphy offered by formation flying: from PROBA-3 to Cosmic Vision", Proc. SPIE 7010, 70101H (2008)
[2] Lamy P.; Damé L.; Vives S.; Zhukov A., "ASPIICS: a giant coronagraph for the ESA/PROBA-3 Formation Flying Mission", SPIE Proc., Volume 7731, pp. 773118-773118-12 (2010)
[3] Richard N. Pfisterer, "Approximated Scatter Models for Stray ,Light Analysis", OPN Optics & Photonics News, October 2011.
[4] E. Renotte et al., "ASPIICS: An Externally Occulted Coronagraph for PROBA-3. Design Evolution", Space Telescope and Instrumentation, Montréal, SPIE 9143 - 87 (2014)
[5] E. Renotte et al., "Design status of ASPIICS, an externally occulted coronagraph for PROBA-3.", Optical Engineering and Applications, San Diego (USA), SPIE 9604 (2015)
[6] C. Galy et al., "Design and Modelisation of ASPIICS Optics", Optical Engineering and Applications, San Diego (USA), SPIE 9604 (2015)
[7] E. Renotte et al., "Recent achievements on ASPIICS, an externally occulted coronagraph for PROBA-3.", Astronomical Telescopes + Instrumentation, Edinburgh, SPIE 9904 – 121 (2016)
[8] C. Baccani, F. Landini et al., "Preliminary evaluation of the diffraction behind the PROBA 3/ASPIICS optimized occulter", Astronomical Telescopes + Instrumentation, Edinburgh, SPIE 9904 – 187 (2016)
[9] F. Landini et al., "Scaled-model guidelines for formation-flying solar coronagraph missions", Optics Letters Vol. 41, Issue 4, pp. 757-760 (2016)
[10] R. Rougeot et al., "Straylight analysis for the hybrid externally occulted Lyot solar coronagraph ASPIICS", Astronomical Telescopes + Instrumentation, Austin, SPIE 10698 (2018)
[11] D. Galano et al., "Development of ASPIICS: a coronagraph based on Proba-3 formation flying mission", Astronomical Telescopes + Instrumentation, Austin, SPIE 10698 (2018)
[12] R. Rougeot, C. Aime, "Theoretical performance of serrated external occulters for solar coronagraphy", A&A 612, A80 (2018)